Journal of Constructional Steel Research 242 (2026) 110344

Contents lists available at ScienceDirect

Journal of Constructional Steel Research

journal homepage: www.elsevier.com/locate/jcsr

Dissipative joints in robustness-related scenarios – Experimental and numerical investigations☆

Tudor Golea [a,*], Roberto Carlevaris [b], Roberto Tartaglia [c], Mario D'Aniello [b], Massimo Latour [d], Vincenzo Piluso [d], Raffaele Landolfo [b], Jean-François Demonceau [a]

[a] Urban and Environmental Engineering, University of Liège, Liège, Belgium
[b] Department of Structure for Engineering and Architecture, University Federico II, Naples, Italy
[c] Department of Engineering, University of Sannio, Benevento, Italy
[d] Department of Civil Engineering, University of Salerno, Salerno, Italy

ARTICLE INFO

Keywords:
Friction joints
Seismic device
Experimental tests
Numerical analysis
Robustness

ABSTRACT

This paper presents the findings of an experimental and numerical study on the full-range behaviour of FREEDAM (FREE from DAMage) beam-to-column joints, with particular focus on their response under column loss scenarios. Two full-scale experimental tests were carried out to evaluate the joint performance under (i) bending moment and (ii) combined bending moment and axial force. The experimental results demonstrated that the sliding resistance and overall response are strongly influenced by the initial bolt preload and by preload loss occurring during the slippage phase, leading to an average reduction of approximately 30% in friction resistance. The tests also showed that the shear failure of the damper bolts governs the ultimate capacity of the joint after damper stroke exhaustion. A simplified component-based spring model was validated against the experimental response, proving capable of reproducing the joint behaviour with satisfactory accuracy when preload loss is properly accounted for. Advanced finite element models were further validated and used to investigate local joint mechanisms and to perform parametric studies on bolt preload effects. These results confirm the suitability of FREEDAM joints for robustness-oriented design and provide validated modelling tools for their implementation in global structural analyses.

1. Introduction

Modern structures are designed to withstand a wide range of identified actions, the intensity of which is typically determined using semi-probabilistic methods or derived from experience. Nevertheless, structural collapses continue to occur, often being triggered by unforeseen and abnormal actions or adverse combinations of loads. Indeed, such unforeseen events can induce local damages that may spread throughout the structure, potentially resulting in a progressive or disproportionate collapse.

To mitigate this risk, design requirements aimed at ensuring an adequate structural robustness have been introduced in modern codes and building regulations. In particular, within the Eurocode framework, EN 1991-1-7 [1] requires that any structure subjected to an exceptional event should not undergo damage disproportionate to the initiating cause. However, although widely recognised as fundamental, robustness – as a design concept – is only introduced in general terms in the current version of EN 1991-1-7 with limited guidance on how to ensure it effectively in the daily design practice. The standard suggests several design strategies intended to achieve minimum robustness levels, but critical issues such as the acceptable extent of damage and the specific accidental scenarios to be considered remain matters of concern for all stakeholders involved in the design, construction, and use of buildings (e.g., engineers, owners, and regulatory authorities).

This lack of consistent normative guidance often leads practitioners to overlook considerations of structural robustness during the design process. To address this gap, significant research efforts have been undertaken over the past decades to derive scientifically grounded design methods for ensuring and evaluating the robustness in steel and steel-concrete composite structures [2–6]. Most studies emphasise the standard-prescribed scenario involving the loss of a load-bearing element (e.g., columns, beam supporting columns, or walls), which

☆ This article is part of a Special issue entitled: 'Connections with Fasteners' published in Journal of Constructional Steel Research.

* Corresponding author.
E-mail address: tudor.golea@uliege.be (T. Golea).

https://doi.org/10.1016/j.jcsr.2026.110344
Received 14 October 2025; Received in revised form 14 February 2026; Accepted 5 March 2026
Available online 12 March 2026

can impose abnormal demands on the structure in terms of resistance and ductility. In such situations, robustness becomes the structure's last line of defence, ensuring survival by mobilising alternative load paths.

Within this context, one of the key research findings allowed identifying the structural joints as critical components, as their performance is essential in enabling the development of catenary actions as the mechanisms that allow the structure to reach a new state of equilibrium under large displacements and deformations [2–4,7].

Moment resisting frames (MRFs) equipped with dissipative FREE from DAMage (FREEDAM) joints can be considered as highly resilient structural systems. Their primary advantage lies in the ability to confine post-earthquake rotation demands within specific, easily replaceable components, enabling a rapid and cost-effective restoration of the structure's pre-event performance through targeted and limited interventions [8].

These joint solutions were developed within the FREEDAM research project [8], and relevant investigations have demonstrated their high potential to minimise earthquake-induced damage in seismic-resistant steel structures, thereby preserving the functionality of buildings even after severe seismic events. The precise control over the stroke and resistance of the friction dampers equipping the beam-to-column joints, combined with the standardised configuration of the friction damper kits, enables the design of connections in seismic-resistant MRFs capable of accommodating large rotation demands typically associated with major earthquakes, with seismic-input energy dissipated through frictional sliding. In addition to friction damping, once the end-of-stroke limit state of the dampers is reached, plasticity developing in plate components engaged in bearing can be seen as an additional energy-dissipating mechanism and provides a reserve of strength and ductility, particularly beneficial in robustness-related loading scenarios.

The robustness of this new connection typology has been previously investigated primarily through analytical and numerical approaches, partially validated against a few experimental tests performed on scaled-down joint specimens [9]. An initial study examining the robustness of MRFs under vehicular impact revealed that the FREEDAM joints can significantly enhance the structural performance compared to conventional joints used in similar frames [10]. The study concluded that, for most of the considered vehicle collision scenarios, no additional structural reinforcement was necessary; however, the replacement of the friction pads in the dampers would be required to fully restore the structural performance.

Further investigations on steel frames incorporating these dissipative joints also demonstrated a satisfactory structural response under column loss scenarios [11–13]. However, findings from previous numerical and analytical studies [12] drew attention to a potential vulnerability associated to the brittle bolt shear failure which can occur once the dampers' stroke is reached, limiting the overall ductility of the joints.

The real-world applicability of FREEDAM connections is currently being demonstrated as a worldwide first through the RFCS DREAMERS pilot project, which involves the construction of a seismic-resistant building on the campus of the University of Salerno [14]. The demonstration building incorporates FREEDAM connections in the perimeter MRFs serving as a seismic-resistant structural system and extends the use of "free-from-damage" technology to non-structural components such as the façade elements, partition walls and the false ceilings by using innovative connecting details assuring low-damage systems suitable for buildings in seismic areas. The building has thus been designed as a low-damage structure capable of meeting the inter-storey drift demands associated with severe seismic events.

Beyond seismic performance, which was considered the primary design objective, structural robustness has also been explicitly addressed as a critical design criterion. Emphasis was placed on the structural response of the perimeter MRFs equipped with FREEDAM joints subjected to an accidental column loss at the base floor. Given that a reliable characterisation of the joints is essential for assessing the structural robustness under such conditions, this paper presents valuable experimental insights into the full-range behaviour of FREEDAM joints.

To this end, real-scale double-sided joints identical to the ones incorporated in the DREAMERS demonstration building were tested up to failure under two distinct loading protocols: monotonic bending (Test 1) and a quasi-static virtual column loss scenario (Test 2). The acquired experimental evidence enabled the validation of an advanced finite element (FE) model and a simplified spring model, generically called the "two-spring model" (2SM) [9]. The advanced FE model was used to widen the investigation of the local response of the tested joints as well as to perform a parametric study aiming at understanding the role of bolt preload on the robustness of the examined beam-to-column joints. Concerning the 2SM, its validation against experimental data supports the applicability of the Component Method of EN 1993-1-8 [15] for characterising the FREEDAM joints and paves the way forward for performing simplified yet reliable global frame analyses that account for the response of these joints under robustness-related loading scenarios [11,12].

2. Experimental program

2.1. General overview of the performed tests

Two experimental tests were carried out on real-scale, double-sided beam-to-column FREEDAM joints representative of the connections adopted for a MRF located along the perimeter of the demonstration building constructed in the framework of the DREAMERS RFCS project. More precisely, the tested specimens replicate an internal joint connecting the IPE450 beams to the HE400B columns on the 1st and 2nd floors of the perimeter frames, as illustrated in Fig. 1.

The performed tests aimed at characterising the full-range behaviour of FREEDAM joints under two distinct loading conditions: i) monotonic bending (Test 1), and ii) a combination of bending moment and axial force simulating a hypothetical column loss scenario (Test 2). A quasi-static loading protocol was applied in both tests, enabling precise control of the experimental conditions and the acquisition of accurate, noise-free measurements that provided valuable insights into the global and local response occurring within the FREEDAM joints.

Although the experimental program addressed loading configurations inducing tensile action in the friction damper, the response of the joint under compression-dominated loading scenarios can be qualitatively assessed based on the mechanical characteristics of the FREEDAM connection. The friction damper provides symmetric resistance in tension and compression, and its resistance is intentionally calibrated to remain significantly lower than the compressive resistance of the beam flange and associated joint components. Therefore, the damper is expected to govern the joint response under both sagging and hogging bending conditions.

2.2. Test specimens

As depicted in Fig. 2, the two specimens consisted of two IPE450 beams connected to a central HE400B column using a FREEDAM connection equipped with the standardised friction damper D1 [8]. All structural elements (i.e., beams and columns) and plate components of the dissipative connections were fabricated using S355 steel, except for the vertical rib of the haunch, which was made of AISI 304 stainless steel. The joint components were assembled using grade 10.9 bolts, with diameters ranging from M16 to M24 in accordance with the standardised joint solution [8].

The global specimen dimensions were selected so that the lengths of the connected beams would be close to the mid-span of the beams employed in the actual building. However, due to space limitations and testing equipment constraints, the span of Specimen 1 was set to 5 m, slightly shorter than the actual 6.048 m span of the considered MRF (see Fig. 1a). Despite this discrepancy, the chosen dimension was deemed acceptable since (i) the span difference would not affect the response of

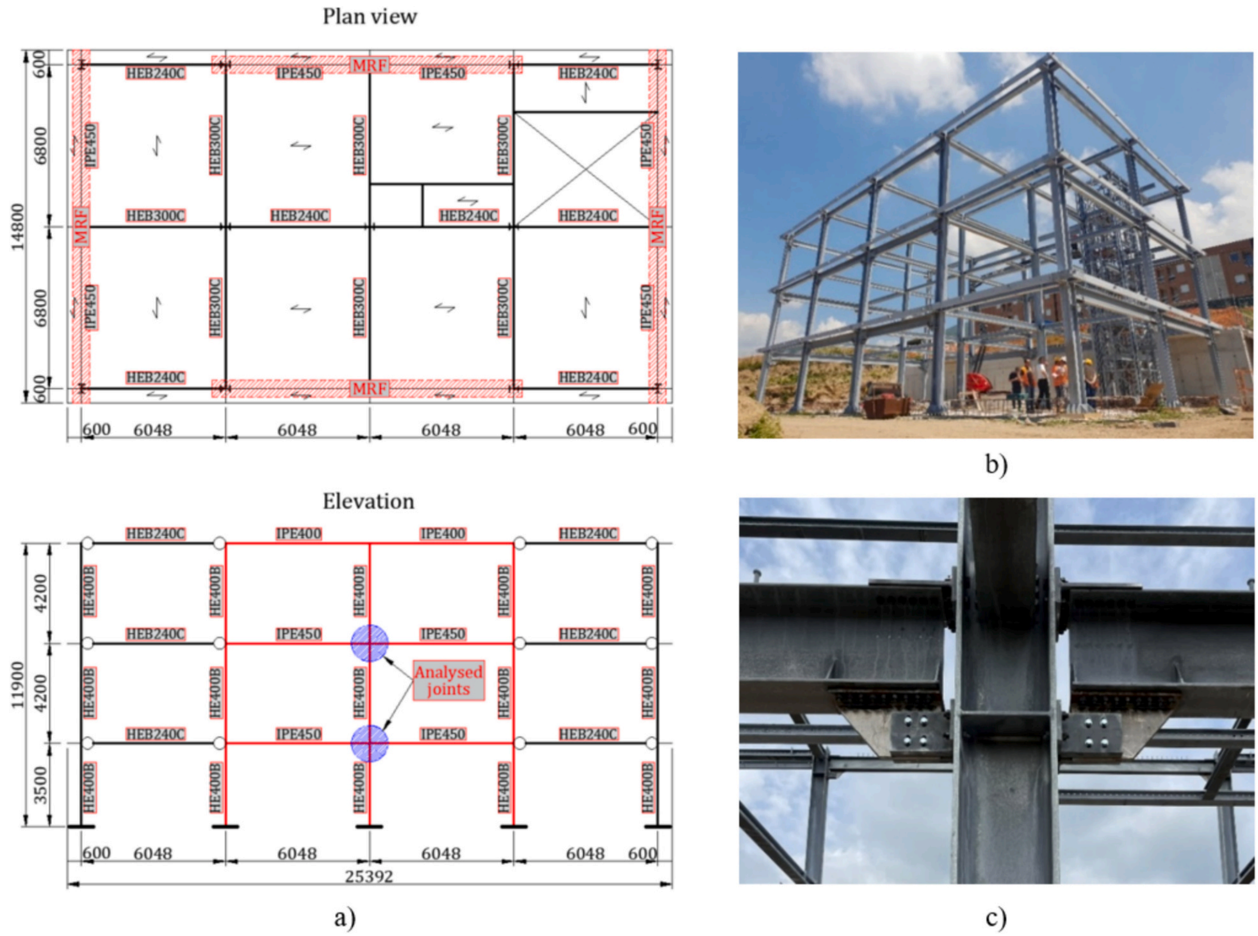

Fig. 1. – General views of the DREAMERS building and investigated joints: a) Plan view and elevation; b) Building under construction; c) Analysed joint within the perimeter MRF.

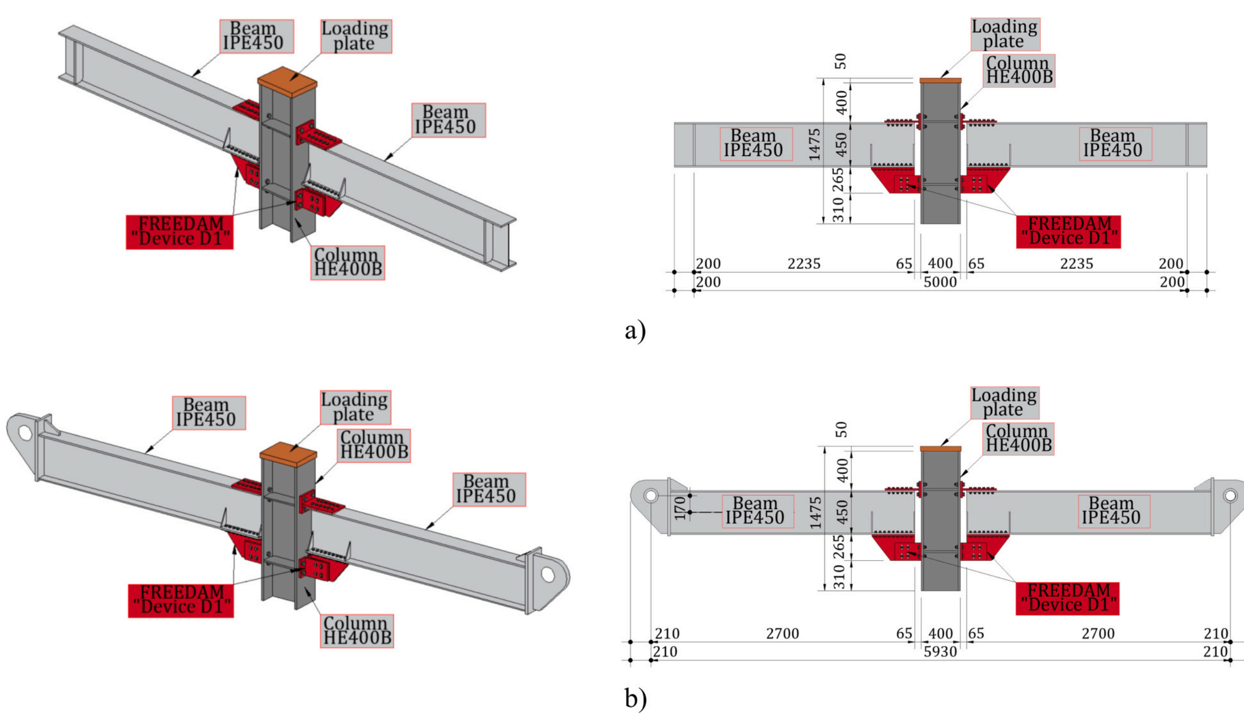

Fig. 2. – Test specimens: a) Specimen 1; b) Specimen 2.

the investigated joint, and (ii) the beam shear deformations remain negligible under the applied loading.

Test 2 aimed at reproducing the actual response of the FREEDAM joint subjected to a column loss scenario with account for the surrounding structure. Consequently, the span of Specimen 2 was set to 5.93 m (see Fig. 2b), which closely matches the span of the perimeter MRF. Additionally, since replicating the lateral restraints provided by the surrounding structure was impractical under laboratory conditions, emphasis was given to the boundary conditions ensured by the test rig. The main objective was to allow the development of catenary action in the beams of the test specimen and to ensure a smooth transition from a bending (flexural) phase to a tensile (catenary) phase, replicating the behaviour expected under an actual column removal scenario. This was achieved by calibrating the hinge locations at the beam ends, where the specimen was connected to the test rig providing both vertical and horizontal restraints.

In particular, the vertical position of the end pins was determined through a fine-tuning process supported by preliminary numerical analyses, aimed at reproducing the expected joint response in the perimeter MRF subjected to a central (base floor) column loss. Assuming rigid axial restraints at the supports, the analysis led to defining a pin eccentricity of 170 mm with respect to the beam axis, as illustrated in Fig. 2b.

Both test specimens were manufactured to reproduce the actual performance of the joints used in the DREAMERS building, designed to fulfil the ULS and SLS requirements. The sliding resistance of the friction damper was calibrated in the design phase to obtain a corresponding joint bending resistance $M_{j,Rd} = 181$ kNm by adjusting the design preload of the bolts clamping the friction pads ($F_{p,d} = 79.3$ kN). The design moment (sliding) resistance of the joint was calculated as:

$$M_{j,Rd} = \mu_{dyn,k} n_s n_b \frac{F_{p,d}}{\gamma_{creep}} z \tag{1}$$

where $\mu_{dyn,k}$ is the characteristic dynamic friction coefficient taken as 0.53, n_s is the number of friction surfaces, n_b is the number of preloaded bolts clamping the damper, $F_{p,d}$ is the design bolt preload, and z is the lever arm equal to 620 mm for the tested joints. The γ_{creep} safety factor accounts for the loss of the initial bolt preload due to relaxation (creep) phenomena and is taken as equal to 1.15 [16] with the aim of compensating for the losses in 50 years.

To apply the targeted preload to the damper M16 bolts of the test specimens, the torque method was employed according to EN 1090–2 [17]. A series of 5 tests was conducted on bolts from the same production batch as the ones used in the tested specimens to determine the k-class of bolts ($k_m = 0.1443$) used for computing the required torque to be applied to reach the target preload.

Therefore, the value of the target preload applied to the friction damper bolts was determined as:

$$F_p = \frac{F_{p,d}}{\gamma_{creep}} = \frac{79.3}{1.15} = 69 \text{ kN} \tag{2}$$

and the corresponding torque to be applied through the torque method was set according to the prescriptions of [17] as follows:

$$M_r = k_m d F_p = 0.1443 \bullet 16 \bullet 69 = 159.3 \text{ kN} \tag{3}$$

This torque was applied in two steps. In the first step, all bolts were tightened to approximately $0.75M_r$, and a torque equal to $1.1M_r$ in the second step was applied as prescribed by [17]. Therefore, the final value of the target preload applied to the damper bolts reached the value of $1.1F_p = 75.8$ kN. During Test 2, the evolution of bolt preload was monitored with strain gauges installed in two damper bolts. The measurements of the initial bolt preload applied by the torque method confirmed the accuracy of the adopted tightening method.

2.3. Test layouts and instrumentation

The test under monotonic bending (Test 1) was conducted using a simple setup consisting of restraining frames and a support system equipped with rollers, which allowed free horizontal displacement of the specimen's extremities. To prevent lateral-torsional buckling (LTB) of the beams – an instability mode observed in previous studies under similar loading conditions [9] – lateral restraints were installed at a distance of 1.0 m from the column axis. A hydraulic actuator with a 2000 kN capacity and a 400 mm stroke length was used to apply a vertical load at the stiffened top end of the column, as shown in Fig. 3.

As shown in Fig. 4, the setup for Test 2 consisted of an assembly of restraining frames and a horizontal in-plane restraining system composed of transfer beams and columns anchored to the laboratory's reinforced concrete floor. This system allows transferring the membrane forces developing in the beams during testing directly to the reaction floor. Pinned supports equipped with radial bearings were placed at the specimen's ends to allow frictionless in-plane rotation. The reaction frame supporting the hydraulic actuator and the in- and out-of-plane restraining systems were securely anchored to the reinforced concrete reaction floor using pretensioned high-strength anchor rods.

In both tests, the quasi-static vertical load was continuously monitored using a load cell positioned between the hydraulic actuator and the top of the column (loading plate). A load button with a convex contact surface was placed between the actuator and the column head to ensure a proper load transfer and maintain the alignment between the applied force and the column's axis.

As indicated in Fig. 5a, Specimen 1 was instrumented with ten Linear Variable Displacement Transducers (LVDTs 01 to 10) to capture both global and relative displacements. Vertical and horizontal global displacements were measured using LVDTs 01,02, and LVDTs 09,10, respectively, while LVDTs 03 to 08 recorded relative displacements between different components of the joint. Additionally, to monitor the rotations of the beam-to-column connections as well as the potential in-plane tilt of the column, three inclinometers (IMs 01–03) were installed at the end of each beam adjacent to the connection and on the column web.

Fig. 5b shows the instrumentation setup used to capture the response of the FREEDAM joint subjected to a virtual column loss during Test 2. In addition to the measuring devices used in Test 1, two extra LVDTs (11−12) were installed at the mid-span of the beams to measure vertical displacements. Two additional inclinometers (IMs 04–05) were positioned near the beam ends, close to the lateral restraints, to estimate any potential horizontal displacement of the restraining system. Eighteen strain gauges (SG 01–18) were mounted on the flanges and webs of the beams to measure the axial forces developing in the restrained beams resulting from the catenary action. Furthermore, additional strain gauges were installed on two M16 damper bolts (one per connection) to monitor the evolution of the preload into the damper bolts throughout the test.

2.4. Experimental results

2.4.1. Material properties

The properties of steel materials used for the constitutive parts of the test specimens were determined by tensile tests performed on coupons extracted from profiles/plates coming from the same production batch as the elements of the test specimens. Table 1 summarises the mechanical characteristics of the tested materials according to ISO 6892-1:2019 [18].

Tensile coupons were not available for the AISI 304 stainless steel used for the vertical rib of the haunch and for the grade 10.9 high-strength bolts employed in the joint assembly. Therefore, the mechanical properties adopted for these components were taken as nominal values according to EN 10088–2 [19] for AISI 304 stainless steel and EN ISO 898-1 [20] for grade 10.9 bolts. Accordingly, for the AISI 304

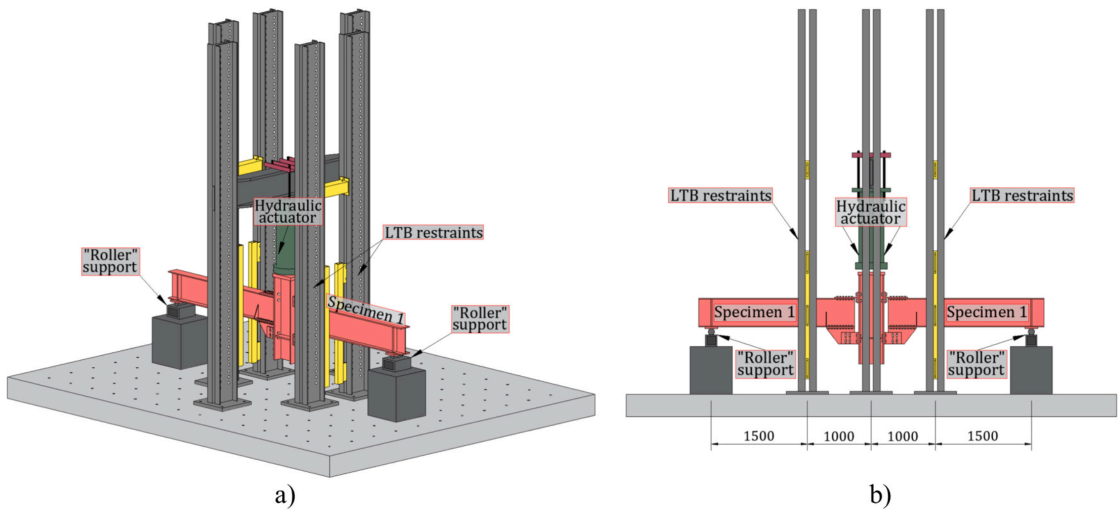

Fig. 3. – Test layout for Test 1: a) 3D view; b) Elevation.

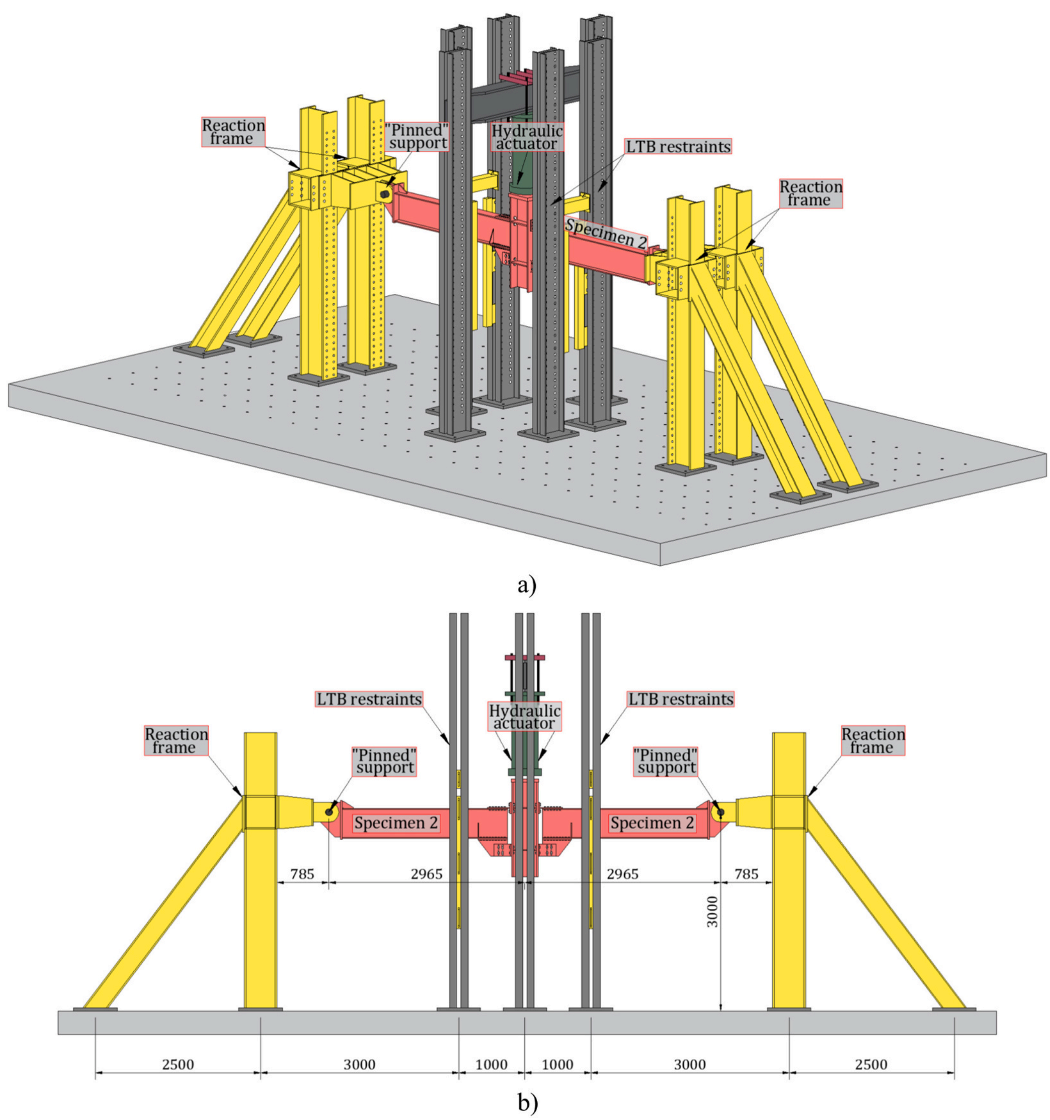

Fig. 4. – Test layout for Test 2: a) 3D view; b) Elevation.

stainless steel, the 0.2% proof strength ($R_{p0,2}$) and the tensile strength (R_m) were taken as $R_{p0,2} = 210$ MPa and $R_m = 520$ MPa with a Young's

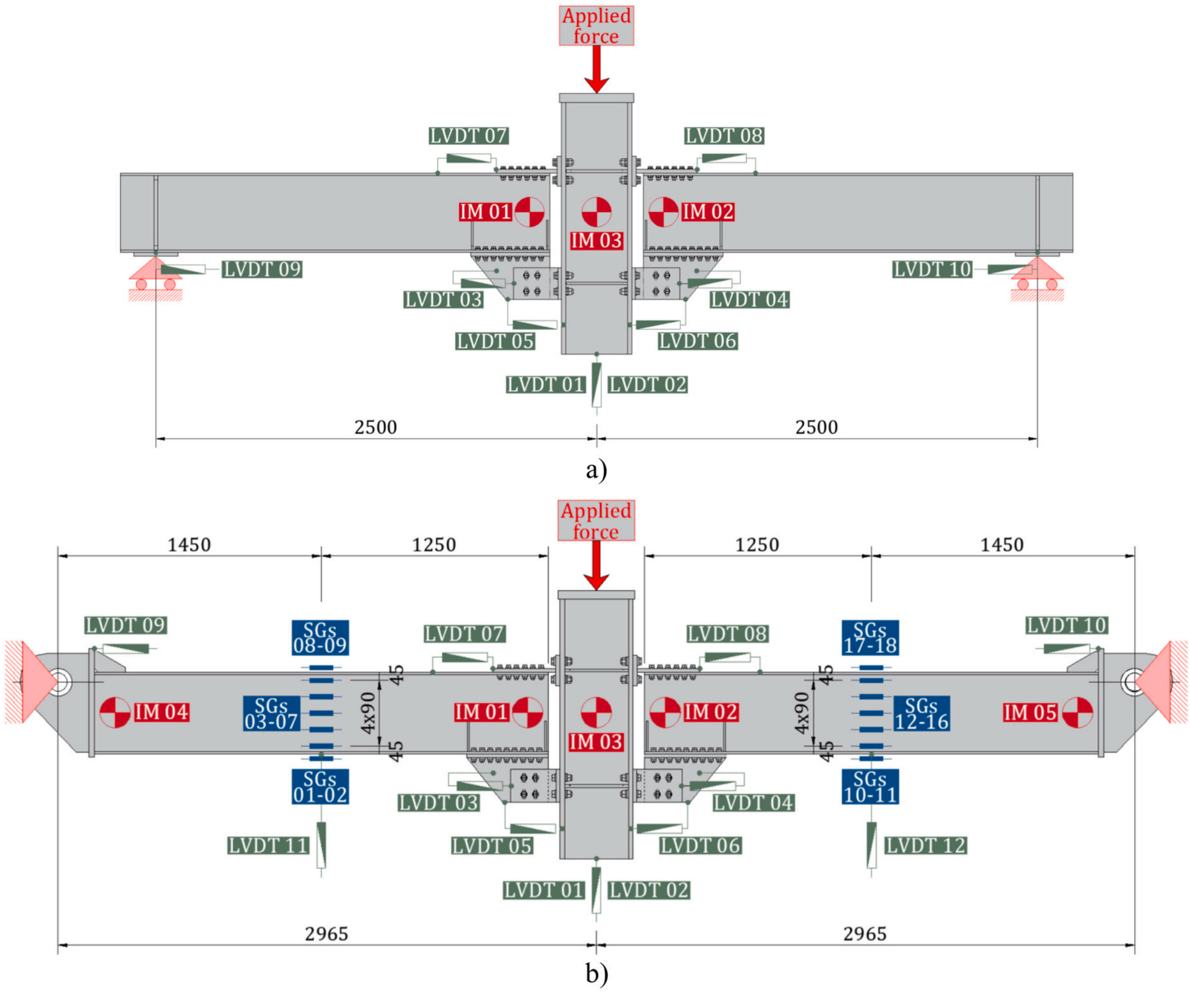

Fig. 5. – Tested specimens and measuring instrumentation: a) Specimen 1; b) Specimen 2.

Table 1
Mechanical properties from steel coupon tensile tests.

Element	Plate	$R_{p0,2}$ (MPa)	R_m (MPa)	A (%)
HE400B	web	474.5	596	24.2
	flanges	415.4	571.3	30.9
IPE450	web	474.1	595.9	24.7
	flanges	456.4	587.8	27.5
Plate 25	25 mm	389.6	558.6	33.6
Plate 20	20 mm	426.8	514.6	34.4

modulus $E = 200$ GPa. For the high-strength grade 10.9 bolts, the nominal values $R_{p0,2} = 900$ MPa and $R_m = 1000$ MPa with $E = 200$ GPa were adopted.

These material properties were adopted consistently in both the simplified and advanced finite element models introduced hereafter.

2.4.2. Test 1 - FREEDAM joint subjected to monotonic bending without axial restraints

Fig. 6a shows the applied force versus the column's vertical displacement curve measured during Test 1, where pure bending was applied to the specimen. The experimental curve, along with real-time observations of the specimen's response, indicates that the sliding resistance of the two connections (left and right) was not reached simultaneously.

Specifically, the results reveal a 7% difference in the sliding resistance between the two connections (see Fig. 6b), with slippage in the right connection being initiated under an applied vertical force of approximately $F = 182$ kN, whereas the left connection reached its sliding resistance at approximately $F = 195$ kN. This discrepancy may be attributed to slight variations of the preload applied to the damper bolts, as well as to the random variability of the friction coefficient resulting from the coating of the friction pads' surfaces [21]. However, the measured sliding resistances of both connections fall within the range defined by the design values based on the characteristic values of dynamic and static friction coefficients $\mu_{dyn,k} = 0.53$ and $\mu_{st,k} = 0.69$, respectively.

It should be noted that in-plane rotation of the column was not restrained during the test, as monitoring the horizontal in-plane reactions resulting at the restraint points proved technically unfeasible. This limitation, combined with the differential sliding resistance of the two connections, resulted in a strongly asymmetric response characterised by five distinct stages, as illustrated in Fig. 6a and Fig. 7.

The five stages marked on Fig. 6a correspond to the following particular response phases:

(1) The attainment of sliding resistance of the right connection at approximately 182 kN and a vertical displacement of 8.3 mm. After this point, the vertical displacement increased to 74.6 mm with a significant drop in the applied force (from 182 kN to 114 kN). Since no sliding occurred in the left connection, the left beam-to-column joint remained in its elastic range, and the relative rotation between the left connection and the column's axis was virtually zero (IM 01-IM 03 ≈ 0). Thus, the rotational

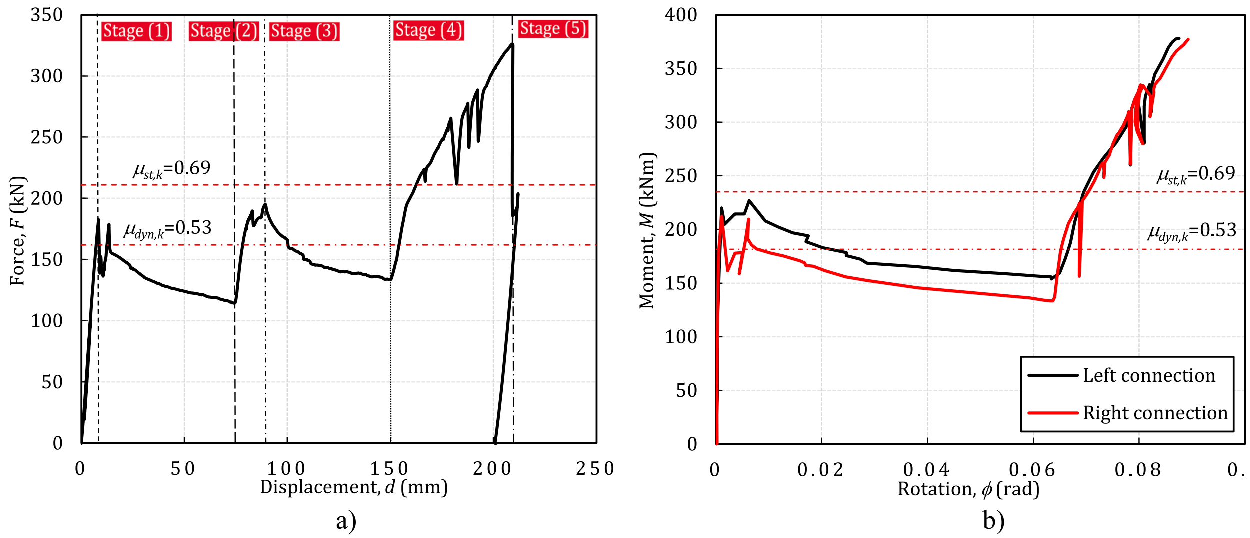

Fig. 6. – Test 1 – Experimental response: a) Vertical load vs. displacement curve; b) Bending moment vs. connection rotation.

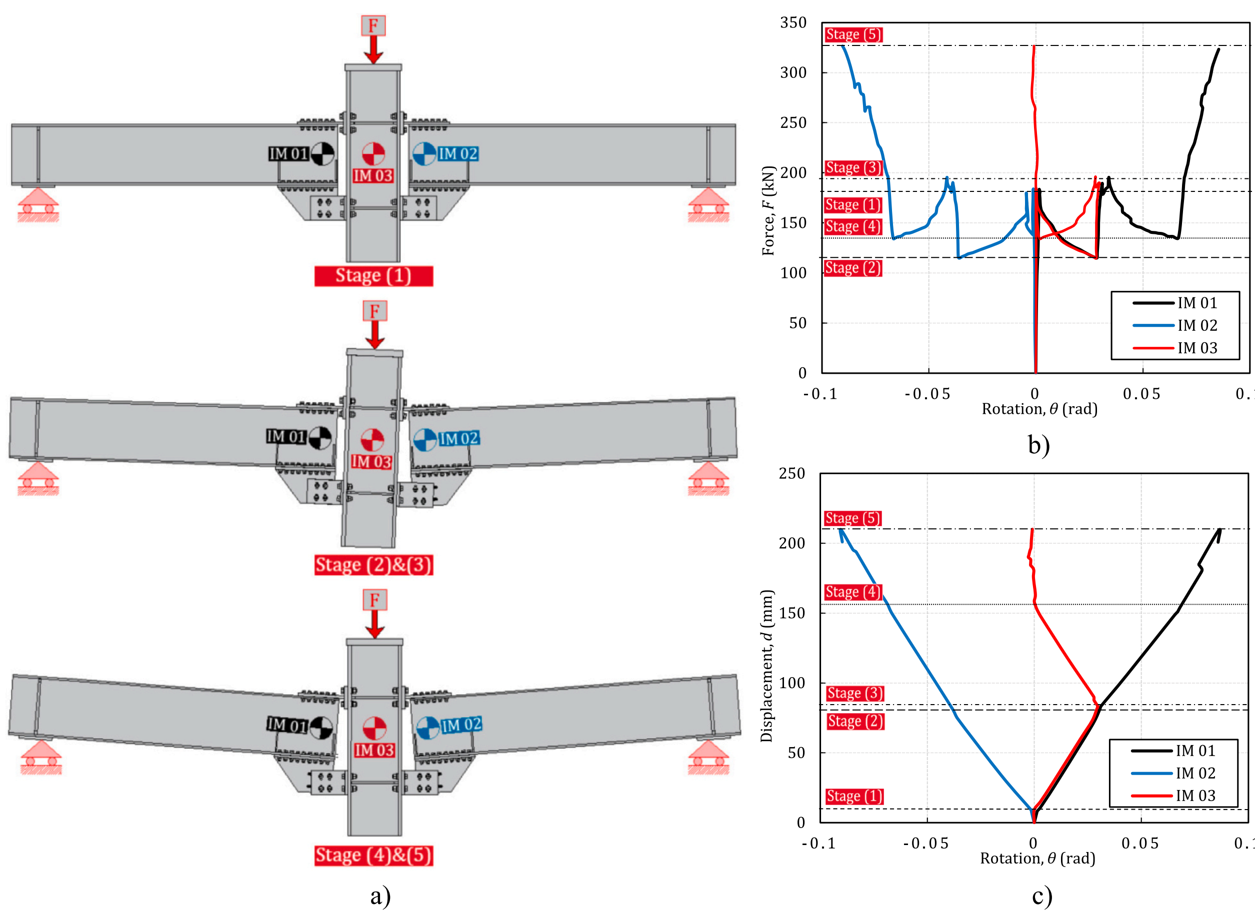

Fig. 7. – Test 1 – Experimental response: a) Response stages; b) Vertical load vs. rotation curve; c) Vertical displacement vs. rotation curve.

response of the left joint at this load step is characterised by the initial stiffness $S_{j,ini}$. This led to the in-plane rotation of the column observed in stages (2) and (3) as shown in Fig. 7a.

(2) The stroke-end limit was reached in the damper of the right connection. The two peripheral M16 damper bolts were gradually engaged in bearing with the haunch plate. The activation of this additional bearing mechanism in the right connection led to the increase of the applied load until reaching the sliding resistance of the left connection.

(3) The peak sliding resistance of the left connection was reached under an applied force of 195 kN and a corresponding vertical displacement of 89 mm. From this instant on, the vertical displacement started once again increasing under a gradually decreasing applied load. The column rotation decreased as well until the column's verticality was restored.

(4) When the stroke-end limit was reached in the left connection at a corresponding vertical displacement of 150 mm, the in-plane rotation of the column decreased to negligible values. Similar to the right connection at stroke capacity, the additional resisting mechanism provided by the bolts engaged in bearing with the haunch induced a further increase of the applied force and both joints (left and right) entered the post-slippage range of response (see Fig. 7b).
(5) The applied force increased continuously until the first failure occurred due to the shear rupture of damper bolts in the left connection. The test was stopped due to safety considerations, yet the brittle failure of the bottom bolt in shear and the excessive plastic deformations at the level of the other bolts (see Fig. 8c) active in bearing in the dampers indicate that the ultimate capacity of the joint was reached at 326 kN and a displacement of 209 mm.

The moment-rotation curves (M-ϕ) for both connections were determined by properly correcting the measured rotations by subtracting (for the left connection) or adding (for the right connection) the in-plane rotation (tilt) of the column. A lever arm $L = 2312$ mm corresponding to the distance between the supports and the mid-thickness of the column's flange was considered in estimating the bending moment at the connection level.

Fig. 6b shows the so-determined M-ϕ curves for both connections. It is evident that the bending moment at which the slippage occurs in both connections falls in the range of the bending resistances estimated based on the characteristic values of dynamic and static friction coefficients.

Fig. 8 shows the deformed shape and the damage pattern of the specimen after the test. As it can be observed, the plastic shear deformations of the bolts depend on their position. In fact, only the outermost bolts closer to the rib edge (see bolts 3 and 4 in Fig. 8b) experienced plastic deformation due to bearing action once the damper's stroke length was reached.

2.4.3. Test 2 - FREEDAM joint subjected to a virtual column loss

In Test 2, the beams of the specimen were axially restrained to simulate the development of catenary actions in the case of a column loss. The force-displacement (F-d) curve reported in Fig. 9a shows that the specimen showed a similar behaviour to the one observed in Test 1 (i.e., the test under pure bending without catenary action). However, due to the presence of tensile forces in the beams, the slippage within the friction dampers occurred at lower values of the applied vertical load. The shape of F-d the curve, as well as real-time observations, indicates that a small difference in terms of slippage resistance between the two connections induced once again an asymmetric behaviour. Overall, the experimental response can be characterised by 5 distinct stages similar to the ones described in the previous section.

The slippage was first observed in the left connection for an applied load of approximately 130 kN and a corresponding vertical displacement of 8.7 mm (1). After reaching the damper stroke-end limit state in the left connection (2), the applied force increased up to approximately 141 kN, the load at which the slippage initiated in the right connection (3). After the attainment of the stroke capacity of the right connection (4), the applied load increased, reaching 294 kN and a corresponding vertical displacement of 220 mm (5) when the test was stopped once again due to safety reasons. Although the bolt fracture didn't expressly occur in Test 2, the comparison between the deformations observed at the level of the damper bolts (see Fig. 10b) in both tests indicates that the ultimate capacity of the specimen was practically reached as well in the second test. Similar to Test 1, plastic deformations were observed at the level of the upper T-stubs and the haunch in bearing.

Additionally, to explain the decay in the friction resistance of the connections along the slippage plateau, the evolution of the preload in the two instrumented damper bolts (one for each damper) with respect to the connection rotation is shown in Fig. 9b. The experimental evidence indicates a preload decrease of approximately 28% (from 78.6 kN to 56.8 kN) for the left damper (LD) and 30% (from 84.8 kN to 58.8 kN) for the right damper (RD) between the slippage onset and stroke-end limit state. Based on this variation, it can be concluded that the decay in the friction resistance observed in both tests along the slippage phase is strongly related to the bolt preload loss.

The axial force acting in the beams (Fig. 9c) was estimated based on the recordings of the strain-gauges located on the beam axis, i.e., SG05 and SG14 for the left and right beam, respectively. The evolution of beam axial forces correlated with the horizontal in-plane displacements of the lateral restraining system allowed estimating the stiffness of the in-plane lateral restraining system at approximately 110 kN/mm.

The moment-rotation curves shown in Fig. 9d were determined by properly correcting the measured rotations by subtracting (for the right

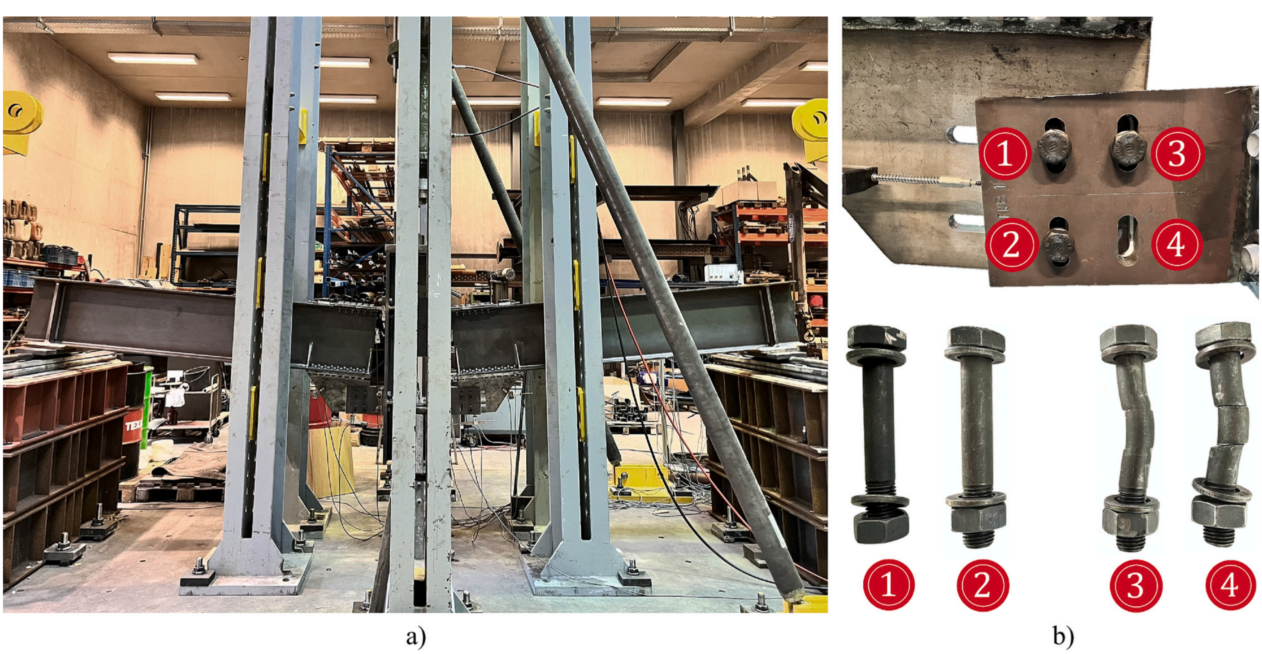

Fig. 8. – Test 1 – Experimental response: a) Deformed specimen after test; b) Friction damper and damage of damper bolts after test.

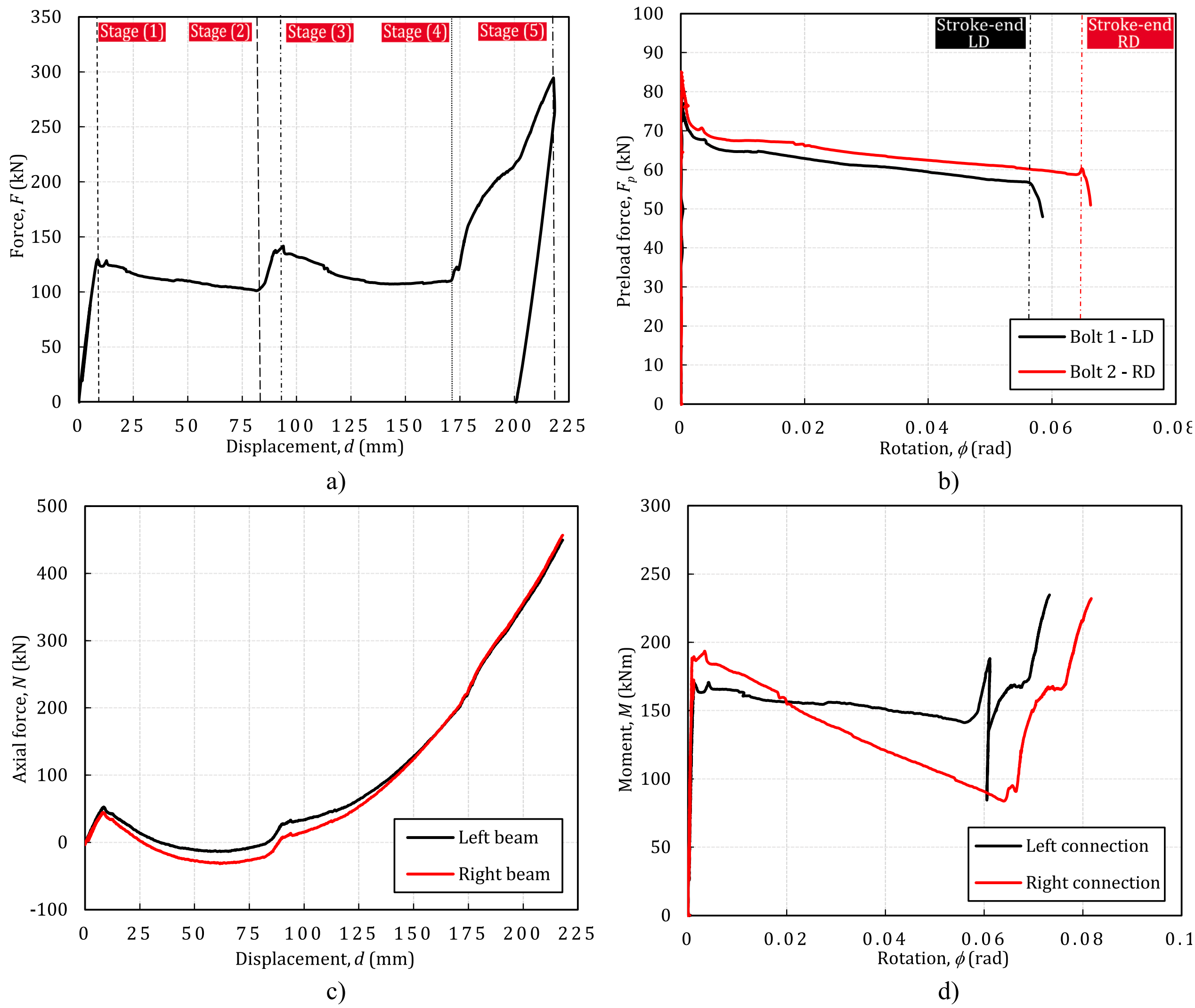

Fig. 9. – Test 2 – Experimental response: a) Vertical load vs. displacement curve; b) Damper bolts preload vs. connection rotation; c) Beam axial force vs. displacement curve; d) Bending moment vs. connection rotation.

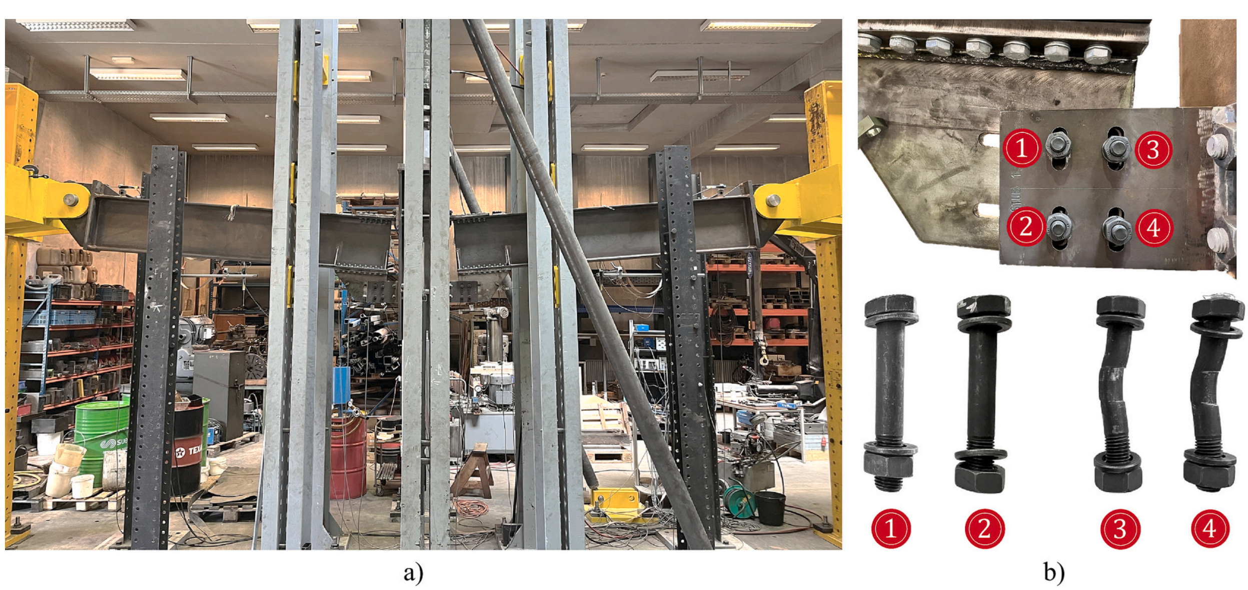

Fig. 10. – Test 2 – Experimental response: a) Deformed specimen after test; b) Friction damper and damage of damper bolts after test.

connection) or adding (for the left connection) the in-plane rotation of the column. The lever arm L for estimating the bending moment at the connection level was taken as the distance between the supports and the mid-thickness of the column's flange (L = 2777 mm). The bending moment acting on the connection was calculated at the beam axis, thus considering the eccentricity $e = 170$ mm of the horizontal reaction at the end supports. Therefore, the bending moment was finally estimated as:

$$M = \frac{F}{2}L - N(e + d) \tag{4}$$

where F is the applied vertical force, N is the axial force in the beam, and d is the corresponding vertical displacement recorded during the test.

Fig. 9d shows the variation of the bending moment computed according to eq. (4) with respect to the rotation of connections (with account for the column tilt). It is evident that the connections were not subjected to the same bending moment along their slippage phase. This difference may be explained by the evolution of the axial force in the beams reported in Fig. 9c.

Since a significant tensile action developed in the beams of the specimen only after the left damper has reached its end of stroke limit state, the left connection is subjected to negligible second order effects during its slippage phase. Therefore, the bending moment acting on this connection during its slippage is mainly induced by the vertical support reaction ($F/2$).

However, this loading state changed with the increase of axial tensile forces once the vertical displacement reached approximately 90 mm. The response of the specimen entered in the catenary action stage, which is characterised by significant second order effects (large displacements) and a steady increase of axial forces in the beams. This combination of changing parameters led to the decrease of the bending moment acting on the right connection during its slippage phase. However, as it can be seen in Fig. 9d, after both dampers reached the end of the stroke limit state, the response of both connections is similar.

The final deformed shape and damage pattern after Test 2 shown in Fig. 10 are rather similar to those observed in Test 1, where similar considerations for the bolts 3 and 4 can be drawn.

3. Simplified modelling of FREEDAM joints

3.1. Overview of the simplified "two-sprig model"

Based on the well-known Component Method codified in EN 1993-1-8 [15], a simplified two-spring model (2SM) was developed and partially validated against experimental evidence by D'Antimo [9] and Santos et al. [22]. The model consists of two extensional springs interconnected by rigid elements, as represented in Fig. 11. An additional rigid shear spring ensures the transfer of shear forces at the beam ends.

The so-built model accounts for the M-N interaction and the behaviour of basic joint components which are characterised by extensional springs with nonlinear behaviour laws (see Fig. 11b-c) derived with the Component Method of EN 1993-1-8 [15]. As demonstrated by Santos et al. [22], the component method can be effectively extended to characterise both pre- and post-sliding behaviour of FREEDAM joints. The plastic range of behaviour for the basic joint components is characterised by a strain-hardening stiffness and an ultimate strength analytically estimated as proposed by Jaspart et al. [23].

To validate the simplified spring model, the experimental tests were numerically simulated using the 2SM with the spring behaviour laws given in Fig. 11b-c combined with classical beam elements in the FINELG FE software [24]. The numerical model overlapped with the configuration of the tested specimens is schematically represented in Fig. 12a-b for Test 1 and Test 2, respectively.

The axial restraints provided in the numerical model through extensional springs in Fig. 12b simulate the in-plane experimental restraining system. The axial stiffness of these restraints was estimated to be equal to 110 kN/mm based on experimental recordings of the axial forces in the beams of the specimen and the corresponding horizontal displacements recorded at the extremities of the specimen.

3.2. Model validation

The comparison between the experimental and numerical responses given in Fig. 13a reveals some inconsistencies between the experimental F-d curve and the prediction of the 2SM in terms of overall curve shape and ultimate capacity of the specimen. The discrepances arise from the approach used in the 2SM for characterising the behaviour of the friction

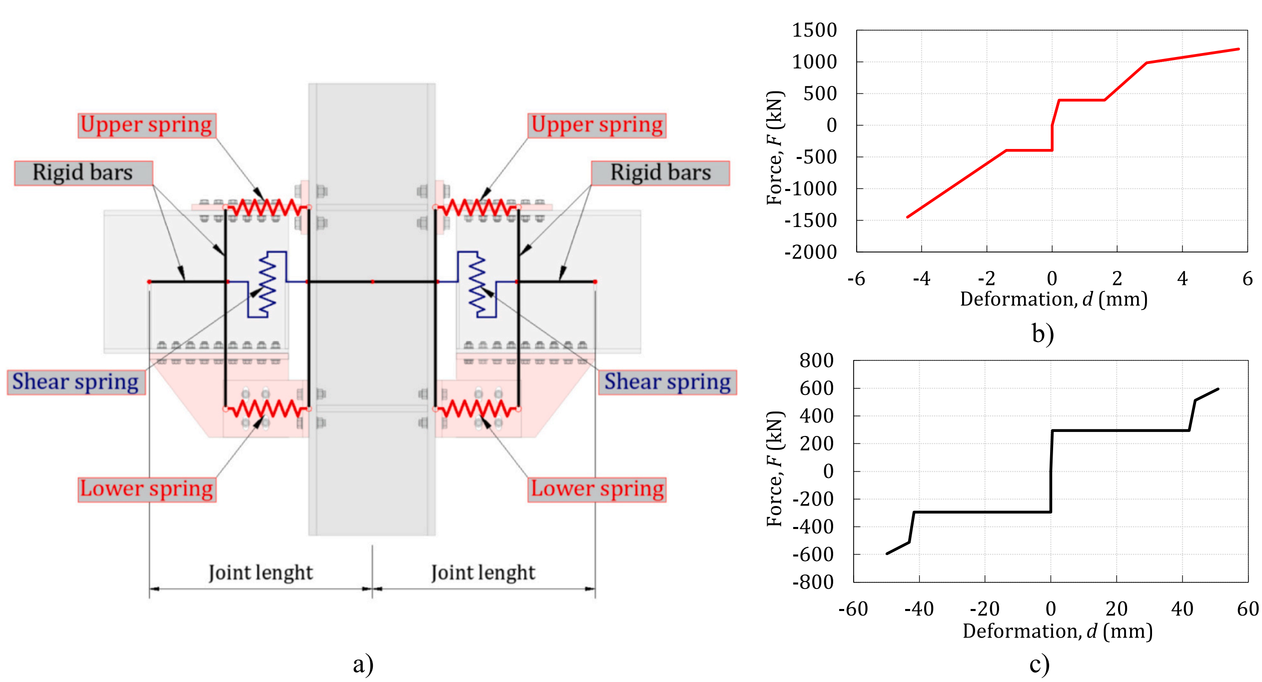

Fig. 11. – Simplified modelling of FREEDAM joints: a) Two-spring model (2SM); b) Upper spring behaviour law; c) Lower spring behaviour law.

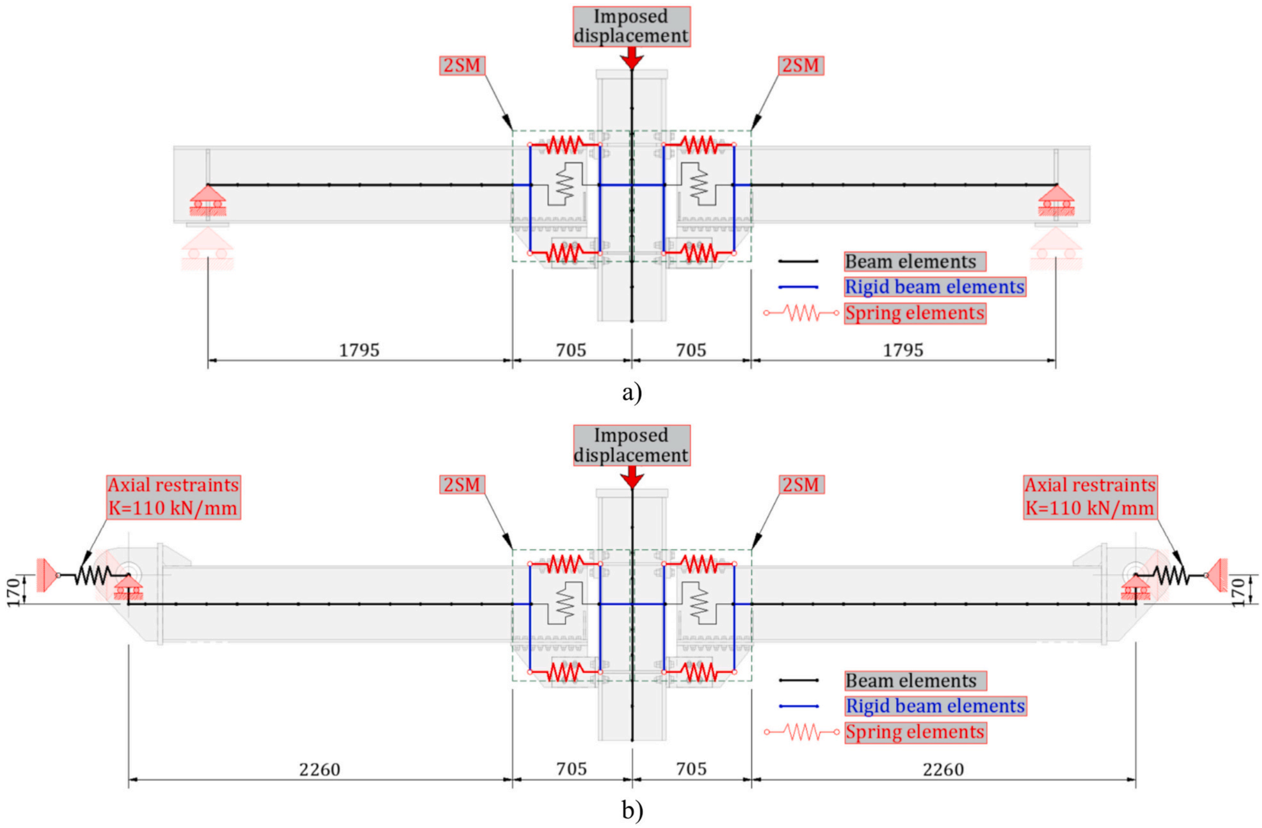

Fig. 12. – Schematic view of the numerical model: a) Test 1; b) Test 2.

damper. The initial modelling approach used to simulate the response of the damper doesn't account for any preload loss that occurs in the preloaded M16 damper bolts along the slippage phase (2SM-w/oPL). This leads to a 6.4% overestimation of the ultimate capacity of the specimen, as well as to an overall plateau-shaped *F-d* curve along the dampers' slippage phase. Nonetheless, experimental observations and measurements taken during Test 2 allowed concluding that an average 29% preload loss was recorded during the slippage phase of the damper.

To account for the expected preload loss, the behaviour law assigned to the lower spring of the 2SM was modified by introducing the 29% preload loss (PL) as a linear decrease along the damper's slippage phase (w/PL behaviour law in Fig. 13b). However, since the resistance decay along the slippage phase due to the preload loss is not an indicative of the joint's robustness but rather a phenomenon that influences mainly the hysteretic energy dissipated under seismic excitation, an additional way of characterising the damper's behaviour was considered for robustness-related investigations. This behaviour law disregards the resistance decay along the damper's slippage phase, yet it accounts for the effects of preload loss on the ultimate resistance of the damper assembly (w/PL(u) behaviour law in Fig. 13b). This modelling approach safely idealises the joint behaviour in the slippage phase through a plateau region, which in turn allows performing stable numerical simulations in robustness-related scenarios accounting for the actual post-slippage behaviour of the joints.

Therefore, three numerical models were built by implementing the preload loss in the M16 damper bolts in three different ways as follows:

– 2SM-w/oPL: the 2SM without any bolt preload loss;
– 2SM-w/PL: the 2SM with bolt preload loss considered as affecting both the friction resistance of the damper during the slippage phase and the ultimate capacity of the joint;
– 2SM-w/PL: the 2SM with bolt preload loss considered only for the ultimate capacity of the joint with a plateau-shaped slippage phase of the dampers.

Fig. 13c reflects the comparison between the predicted and the experimental *M-ϕ* curves for the right and left connections (RC and LC) of the tested joint. Generally, the 2SM model shows a good performance for predicting the full-range behaviour of FREEDAM joints, although the results reveal the model's sensitivity to the characterisation of basic joint components. Indeed, the behaviour law considered for the friction dampers plays a crucial role in achieving accurate predictions in terms of both deformation and strength capacities.

It is evident that to accurately predict the ultimate capacity of the connections, the preload loss in the damper bolts and its inherent effects on the friction resistance should be considered. For both cases where the expected preload loss was considered (2SM-w/PL and 2SM-w/PL(u)), the 2SM model provides predictions with acceptable accuracy for the full-range behaviour of the tested joint, with a notable perfect match between the recorded and the predicted ultimate moment resistance and deformation capacities, both parameters being of key importance for assessing the robustness of the joints.

For Test 2, the comparison between the predicted and the experimental *F-d* curves shown in Fig. 14a highlights the sensitivity of the 2SM to the method used for characterising the behaviour of basic joint components. It is worth noting that the best agreement between the predicted and the experimentally observed response is provided by the numerical model in which the preload loss was considered as occurring along the dampers' slippage phase with inherent effects over the friction and ultimate resistance of the FREEDAM joints (2SM-w/PL).

However, an acceptable prediction is also provided by the numerical model in which the preload loss was considered as affecting exclusively the ultimate strength of the joint (2SM-w/PL(u)) and the slippage phase characterised by a plateau. Although the decay in the applied force

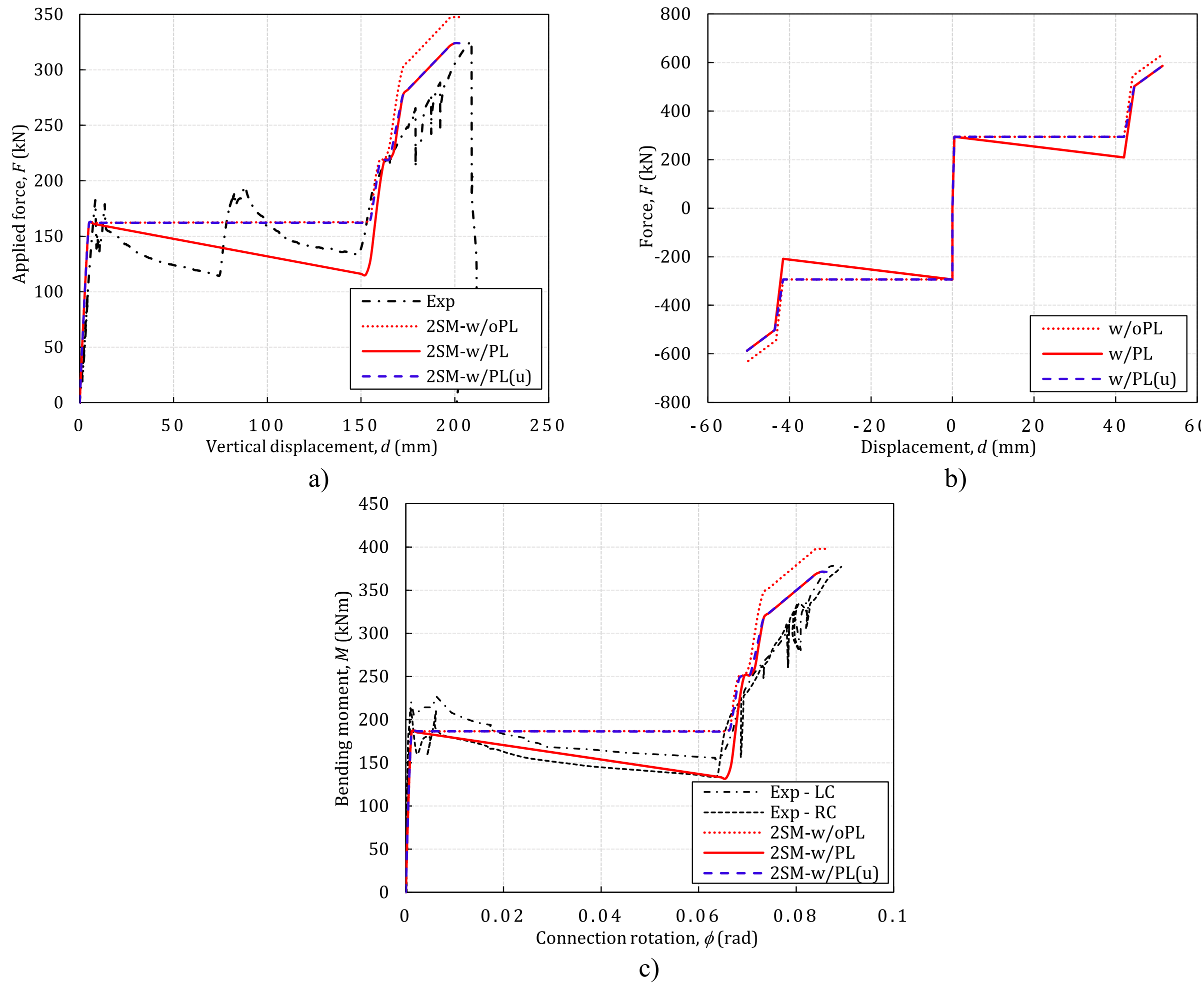

Fig. 13. – Simplified 2SM validation – Test 1; a) Applied force vs. displacement curves; b) Lower spring (damper) behaviour laws; c) Moment vs. rotation curves.

along slippage is not captured, the model provides an identical post-slippage response in terms of stiffness and ultimate capacity as the 2SM-w/PL model.

An overestimation of the specimen's ultimate capacity of approximately 9% is observed for both numerical models in which the preload loss was implemented. This discrepancy may be attributed to the fact that the experimental test was stopped before reaching the actual ultimate capacity of the specimen, which would correspond to the brittle rupture of the damper bolts subjected to shear. Indeed, since the actual failure was not reached during testing, some residual strength should be envisaged. This was highlighted by the perfect agreement between the predicted and actual capacity of the specimen used in Test 1, where the ultimate failure was reached.

Fig. 14b shows the development of beam catenary action during testing and the predictions provided by the three numerical models. It is worth noting that the evolution of beam axial forces seems to be insensitive to the approach chosen to characterise the friction damper with respect to the bolt preload loss.

As previously mentioned, unlike the axial force in the beams, the evolution of the bending moment at the connection level is highly dependent on the specific behaviour of the friction damper. This observation is supported by the results presented in Fig. 14c, where the comparison between the experimental response of the right connection (RC) and the numerical prediction demonstrates the accuracy of the 2SM in replicating the behaviour of the FREEDAM joint under combined *M-N*, provided that the preload loss is appropriately accounted for.

4. Advanced numerical modelling of FREEDAM joints

4.1. Overview of the numerical model

Advanced numerical analyses were performed by means of Abaqus/CAE v. 6.14 [25] by using a Dynamic Implicit quasi-static procedure suitable for low loading rate and non-linear behaviours.

Two loading steps were defined: the first one was used for the tightening of the bolts by means of the “Bolt Load” feature, while in the second step, a downward displacement of the column top was imposed, replicating the action of the jack used in the experimental setup.

Both geometric and material non-linearities were accounted for, respectively, by toggling on the “Nlgeom” option in the step's definition and by using true stress – true strain curves derived from experimental tensile coupon tests (see Table 1). Like in the experimental setup, S355 steel was adopted for the steel plates and profiles, except for the haunch, made of AISI 304 stainless steel. The mechanical properties of the AISI 304 were deducted from the nominal values suggested by EN 10088–2 [19] and reported in Section 2.4.1. All the bolts were HV high-strength bolts grade 10.9 and modelled according to [26], with material properties mentioned Section 2.4.1. As suggested in [26], the equivalent yield stress of bolts was 708 MPa, while the ultimate tensile stress was influenced by the nominal bolt diameter, ranging from 794 MPa to 889 MPa.

Contacts were modelled as an interaction feature by means of surface-to-surface contact by defining every surface separately. Contact properties consist of tangential behaviour with penalty formulation and

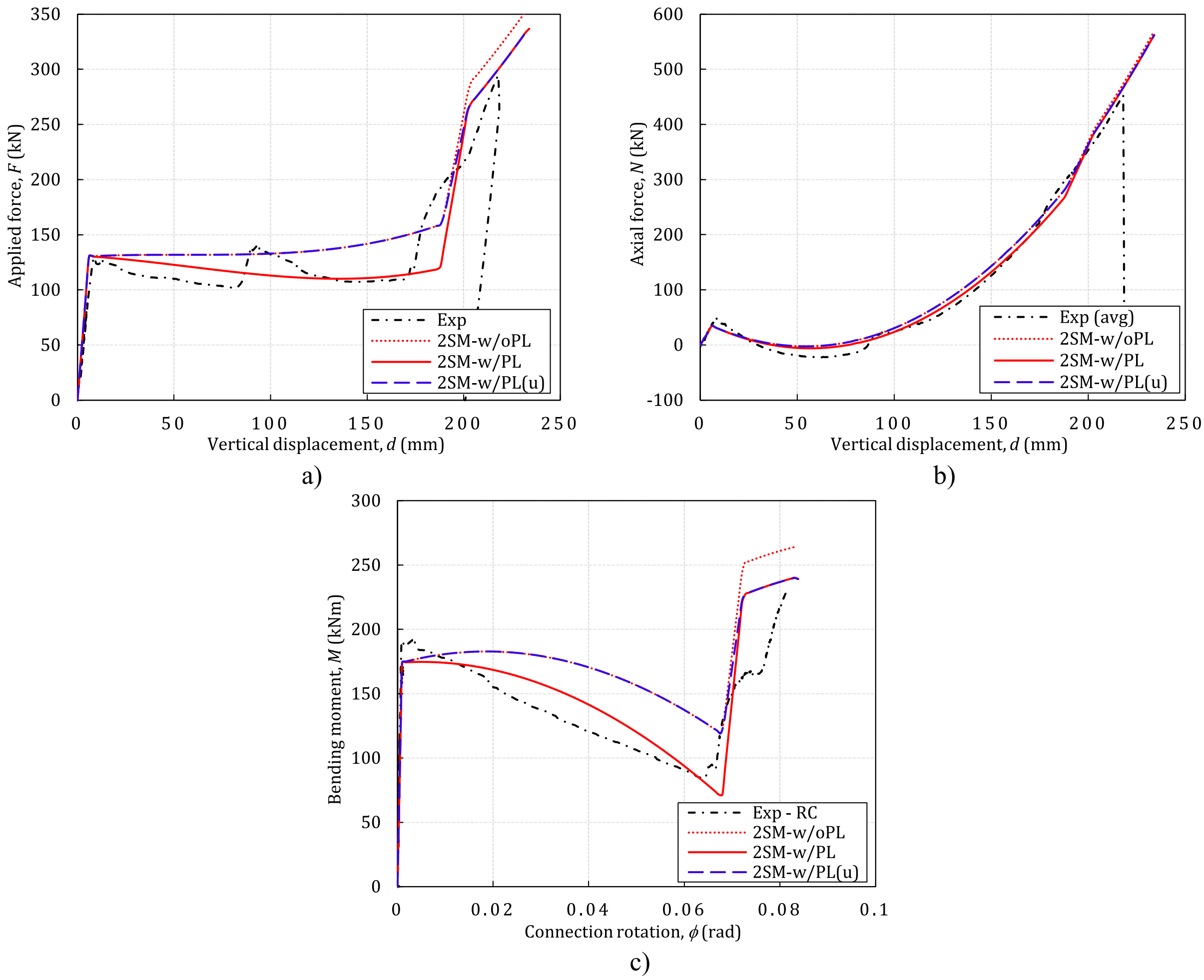

Fig. 14. – Simplified 2SM validation – Test 2; a) Applied force vs. displacement curves; b) Beam axial force vs. vertical displacement curves; b) Connection moment vs. rotation curves.

normal behaviour with pressure-overclosure defined as "hard contact" and allowing the separation after contact. Friction coefficient was set to 0.3 for generic steel-to-steel contact, while the kinematic friction coefficient equal to 0.53 [27] was adopted for the sliding surfaces of the friction dampers. The welds were modelled as tie constraints.

The boundary conditions as well as the imposed displacement were enforced by means of reference points, connected with a rigid body constraint to the points of the respective cross-section in function of the test setup. In particular, the boundary conditions were imposed as follows:

- In the Model for Test 1, each beam's free end was equipped with rollers, allowing them to move horizontally but preventing vertical displacements. Vertical downward displacement is imposed at the top of the column (see Fig. 15a).
- In the Model for Test 2, the boundary conditions adopted for Test 1 were enriched with the addition of horizontal restraints at the beams' free end, modelled as a spring element whose stiffness K is equal to 110 kN/mm – to take into account the deformability of the restraint frame used in the experimental tests. It is worth noting that the reference points at the beams' free ends were placed in correspondence with the pin considering the experimental eccentricity of 170 mm with respect to the centroid of the cross-section (see Fig. 15b).

Linear brick elements with reduced integration (C3D8R) were adopted for all the parts, and the mesh size was selected based on the results of a mesh sensitivity analysis properly performed and discussed

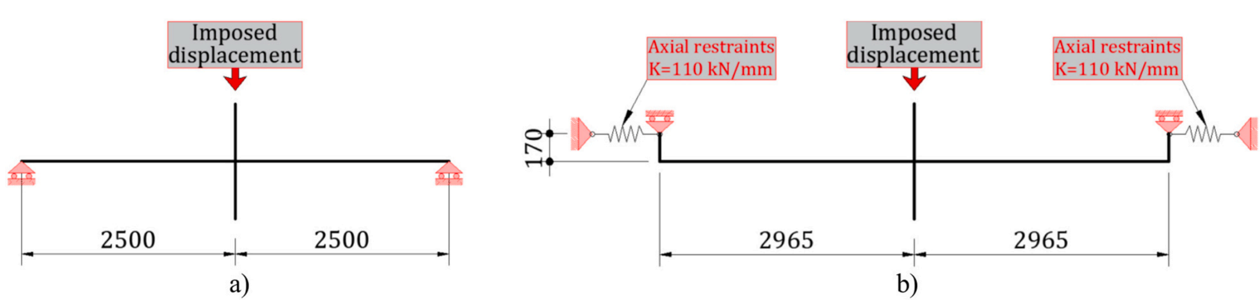

Fig. 15. – Imposed boundary conditions to mimic the experimental tests: a) Test 1; b) Test 2.

in the following paragraph.

4.2. Mesh sensitivity analysis

To optimise numerical accuracy and computational efficiency, a mesh sensitivity analysis was conducted to define the most suitable mesh density for the four main components: the beams, the upper T-stub, the damper bolts, and the haunch.

For each investigated components, the moment-rotation curves and the Von Mises stress value on a selected control point were monitored, changing the mesh density for a reference rotation level (i.e., 2% and 4%). The variation of the mesh density was selected in function of the geometrical dimensions and the expected stress distribution of each component; thus, the following elements' dimensions were investigated:

- Beam: 5, 10, 15, 30, 60 mm;
- T-stub: 1, 5, 15, 20, 30 mm;
- Damper bolts: 0.5, 2, 5, 15, 30 mm;
- Haunch: 2, 5, 15, 30, 50 mm.

As an example, Fig. 16 depicts the investigated configurations changing the T-stub element dimensions (EDs). The results of the mesh sensitivity analysis of all the investigated components are depicted in Fig. 17. As it can be observed for each of the investigated components, the influence of the element dimension on the numerical simulation results was monitored in terms of both moment-rotation curve and the Von Mises stress value. In almost all the investigated cases, the global behaviour of the analysed configuration is almost constant and independent of the mesh element dimension, although some differences can be observed under large rotational values (i.e. larger than 5%). Contrariwise, looking at the local point of view, a variation of the Von Mises stress can be observed. Therefore, a fine mesh with an average size of 2 mm was adopted for the bolts, 5 mm for the T-stub and the haunch, and a 30 mm mesh was used for the beam and all the other joint components.

4.3. Model validation

As anticipated, the experimental tests revealed an unexpected behaviour of the connection, differing from the outcomes of previous experimental tests performed as part of the FREEDAM research project [8]. Specifically, the test did not exhibit a clear plateau for the design bending moment resistance at the onset of the sliding mechanism that characterises this type of joint [24]. Instead, due to micro-defects in the specimen, column boundary conditions, and asymmetry in the friction surfaces, a softening response and asymmetrical activation of the connection were observed. To accurately replicate these experimental findings through FE analysis, geometric imperfections, measured asymmetry, and the actual boundary conditions were incorporated into the numerical model.

Fig. 18a depicts the comparison between the experimental Test 1 and numerical results in terms of applied force – displacement curve and Von Mises stress distribution. To properly model the asymmetric joint performance observed during the experimental test, the damper bolts of the left and right connections were tightened with different values of the preload force F_p – instead of using the design value of 69 kN. The damper bolts of the right friction connection were tightened to 100% of F_p with a 35% loss of preloading during the analysis. Conversely, the damper bolts of the left friction connection were preloaded to 120% of F_p and subjected to 35% tightening loss.

As it can be observed in Fig. 18b, the numerical model was able to accurately reproduce the experimental test results up to very large displacements and to properly simulate the stress distribution within the joint zone.

Fig. 19a depicts the comparison between the Test 2 experimental response and FE numerical results in terms of applied force–displacement curves. It is worth noting that, differently from the previous case, the beam ends were axially restrained in Test 2 so that the normal actions developed in the beams. All the damper bolts were tightened to the design preload force of 69 kN, and a 30% preload loss was imposed. The numerical model was able to accurately predict the joint response in terms of force-displacement curves; indeed, Fig. 19a shows that the numerical curve is in good agreement with the experimental one, and that only at large displacements (i.e. 220 mm) a variation of 15% between the two curves can be pointed out. In line with these results, the comparison of the beams' tensile action further validates the accuracy of the numerical model's predictions.

Fig. 19b presents the Von Mises stress distribution, which is in good agreement with the experimental observations.

4.4. Parametric study on the influence of preload imperfection of the damper bolts

The influence of on-site imperfections with regard to uneven torque of the bolts of the friction device was numerically investigated by means of advanced FE analyses in Abaqus. The study was conducted on two external joints sub-assemblies with geometries and boundary conditions (see Fig. 20a) pertaining to the same DREAMERS frame. This resulted in a beam length of 3.024 m (for a total span length of 6.048 m) and an inter-storey height of 4.2 m. IPE450 and HE400B were adopted, respectively, as beam and column profiles. The column was pinned at the base and equipped with a roller at its top. Bending action on the joint was imposed by means of a controlled displacement of the beam free end, under both monotonic hogging and sagging loading scenarios.

The two external joint sub-models had the same characteristics, except for the equipped FREEDAM device:

- D1–0.3, consisting of FREEDAM Device 1, 4xM16 10.9 damper bolts, with a design bending resistance equal to 0.3 times the plastic

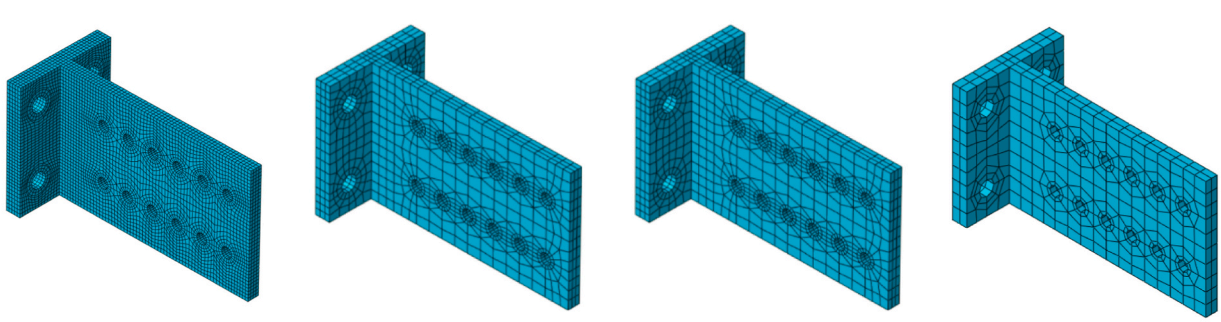

Fig. 16. – Element dimensions used in the mesh sensitivity analysis of the T-stub component.

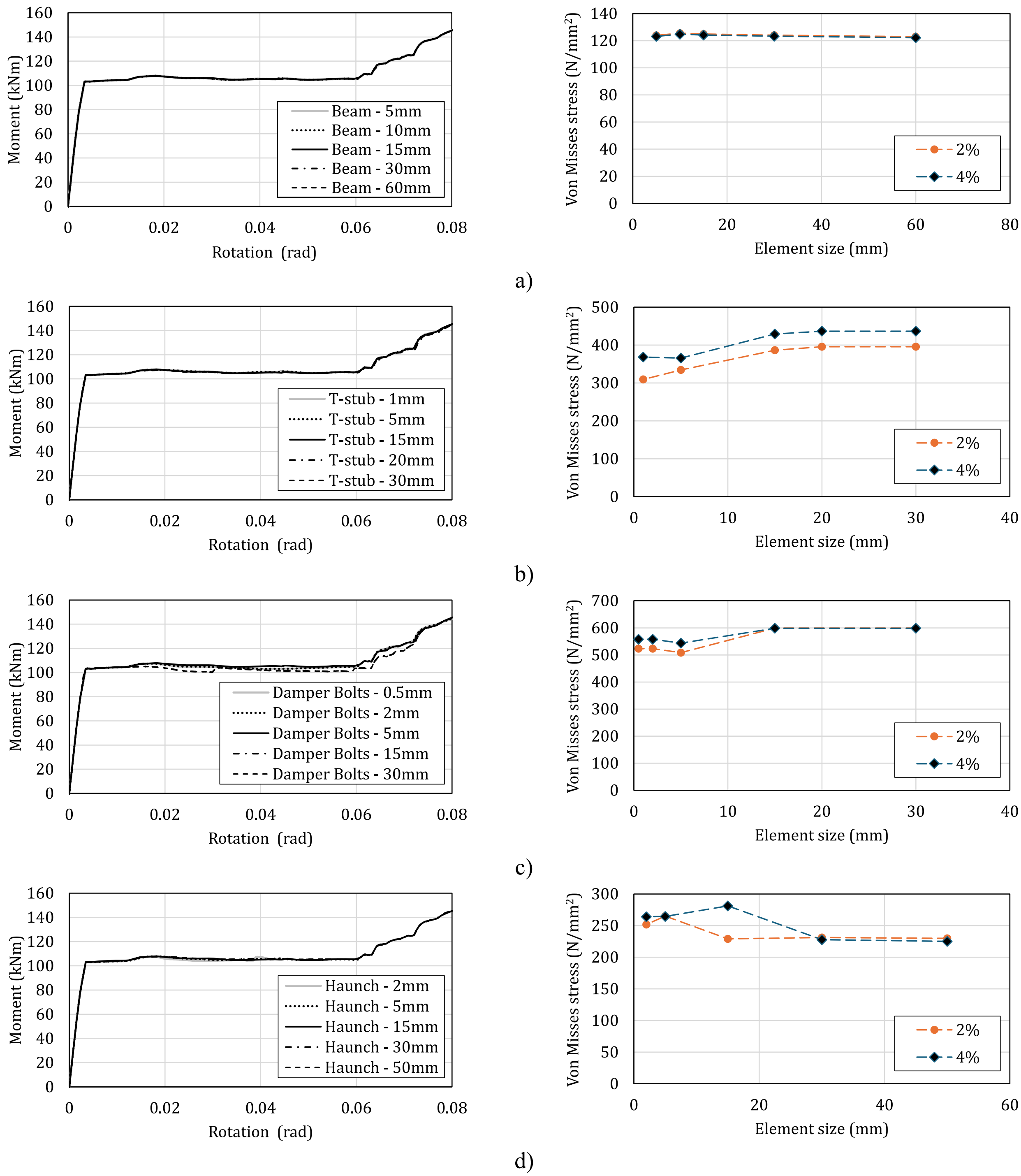

Fig. 17. – Mesh sensitivity analyses results in terms of both moment rotation curve and Von Mises stress: a) Beam; b) T-stub; c) Damper bolts; d) Haunch.

bending resistance of the connected beam: $M_{j,Rd} = 181\ kNm$. Design preload force F_d was equal to 69 kN.

– D2–0.4, consisting of FREEDAM Device 2, 4xM20 10.9 damper bolts, with a design bending resistance equal to 0.4 times the plastic bending resistance of the connected beam: $M_{j,Rd} = 241\ kNm$. Design preload force F_d was equal to 81 kN.

The sensitivity to torque imperfections was investigated by means of nine different preload patterns (named “c00” to “c08”) of the damper bolts. The resultant clamping force acting on the device was kept constant to ensure the same design bending moment resistance of the connection, equal to the number of damper bolts multiplied by F_d. However, each damper bolt is tightened with a torque equal to 70%, 100%, 130% of F_d, depending on the specific preload pattern, since a torque imperfection of +/− 30% was judged to be representative of a real-world scenario.

Table 2 shows the coefficients α_{ij} of the preload for the bolts of each damper according to the preload pattern. The preload of the *i-th* damper bolt according to the *j-th* preload pattern is given by the formula $F_d^i = \alpha_{ij} F_d$, with the naming convention shown in Fig. 20b.

Preload pattern “c00” with damper bolts tightened to the design preload, was used as a reference.

Fig. 21 depicts the results of the parametric investigations in terms of

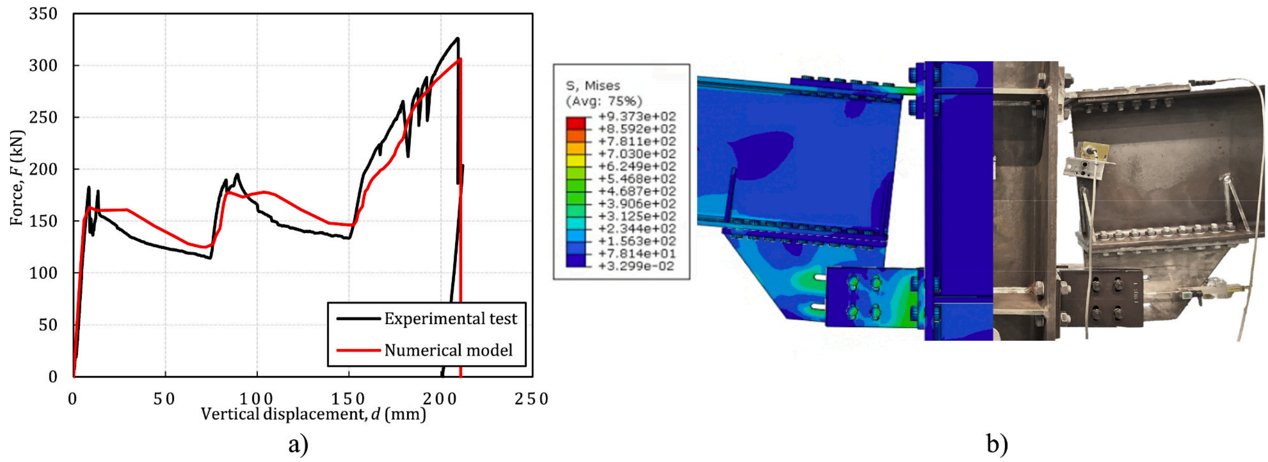

Fig. 18. – Comparison between the numerical and experimental results: a) Force-displacement curves, b) Test deformation and Von Mises stress distribution.

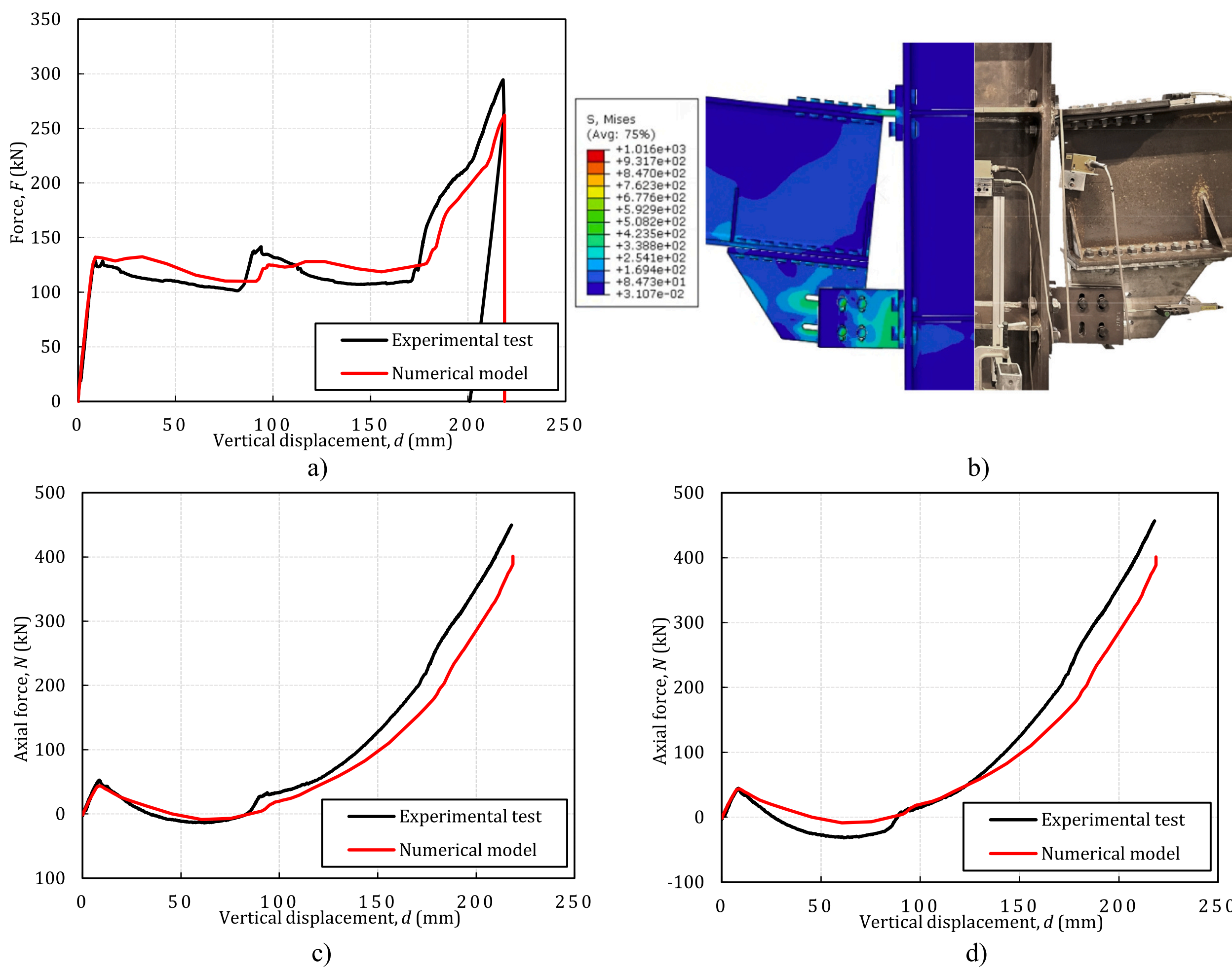

Fig. 19. – Comparison between the numerical and experimental results: a) Force-displacement curves; b) Test deformation and Von Mises stress distribution; c) Right beam axial force-displacement curves; d) Left beam axial force-displacement curves.

the moment-rotation curves. Hogging and sagging bending moments are compared for the sub-assemblies D1–0.3 and D2–0.4. As observed, the torque imperfection does not significantly affect the overall behaviour of the connection, underscoring the high versatility of FREEDAM connections, which remain functional and effective even under unpredicted on-site imperfections.

5. Conclusions

Two large-scale tests were conducted on dissipative FREEDAM joints representative of the connections used in the DREAMERS demonstration building. The full-range response of double-sided beam-to-column joints was experimentally investigated under two loading conditions: (i) monotonic bending (Test 1) and (ii) a virtual column loss scenario (Test

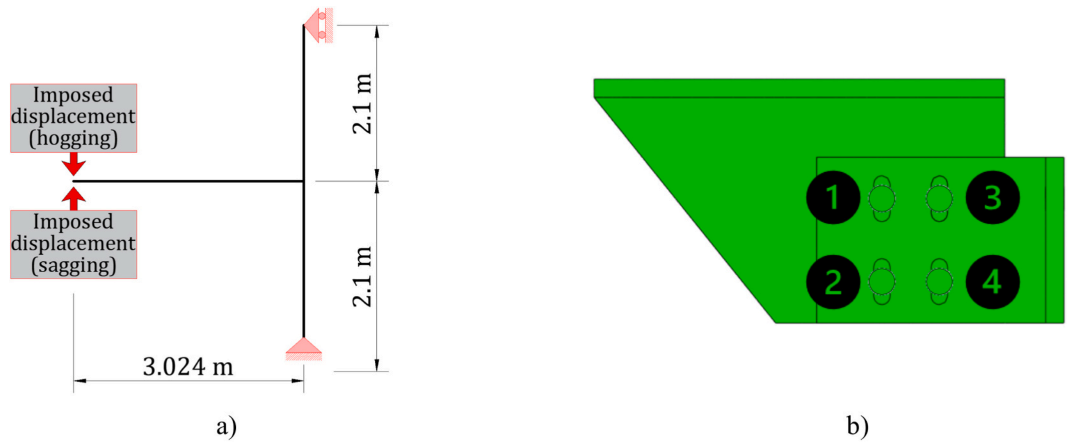

Fig. 20. – Analysed joints sub-assemblies: a) Boundary conditions; b) Damper bolts IDs.

Table 2
Preload coefficient α_{ij} for the bolts of each damper and preload force pattern.

Preload force pattern	Damper Bolt 1 [–]	Damper Bolt 2 [–]	Damper Bolt 3 [–]	Damper Bolt 4 [–]
c00	1.00	1.00	1.00	1.00
c01	1.00	1.30	0.70	1.00
c02	0.70	1.00	1.00	1.30
c03	1.00	0.70	1.30	1.00
c04	1.30	1.00	1.00	0.70
c05	1.30	1.30	0.70	0.70
c06	0.70	0.70	1.30	1.30
c07	0.70	1.30	0.70	1.30
c08	1.30	0.70	1.30	0.70

2).

Experimental evidence highlighted the detrimental effects of the preload loss in the damper bolts during the slippage and their influence on the sliding resistance of the FREEDAM joints under quasi-static loads. Moreover, the results of Test 2 featuring catenary effects revealed the capability of these joints to accommodate high levels of displacements accompanied by the development of membrane forces in the connected beams, confirming their suitability for use in robustness-oriented design strategies where alternative load paths are required. However, the brittle failure observed in the form of bolt shear fracture emphasises the need to carefully consider the joint's ductility and failure mechanisms in the post-slippage phase.

The validation of the simplified 2SM model proved its suitability for numerical studies in which the full-range behaviour of FREEDAM joints is of interest. Moreover, for robustness-related investigations such as simulations of column loss scenarios where the post-slippage response of the joints is critical, the validation of the 2SM model allowed identifying an acceptable compromise between model complexity and accuracy.

The identified modelling solution accounts for an expected preload loss of 29% at the damper stroke-end limit state, which affects both the friction and the ultimate capacity of the joint (w/PL). However, to ensure the convergence of large numerical simulations performed on global structural models, the preload loss can be considered as affecting exclusively the ultimate capacity of the joints (w/PL(u)). Therefore, the slippage phase of the damper's response can be defined as a plateau, and the effects of the preload loss can be integrated into the estimation of the damper's ultimate resistance. This modelling approach eliminates the need for introducing response regions with negative stiffness, which in turn facilitates the convergence for numerical solvers with a marginal influence on the overall accuracy of the results when the post-slippage response of FREEDAM joints is of concern.

As a complement to the experimental campaign, FE models were carefully developed and validated. The advanced numerical models were capable of accurately predicting the experimental behaviour of the tested specimens, with the connections subjected to pure bending moment (Test 1) and to combined bending moment and tensile action (Test 2). In particular, the models captured the asymmetric behaviour of the joint. The numerical results are consistent with the experimental findings, both in terms of moment–rotation response and global

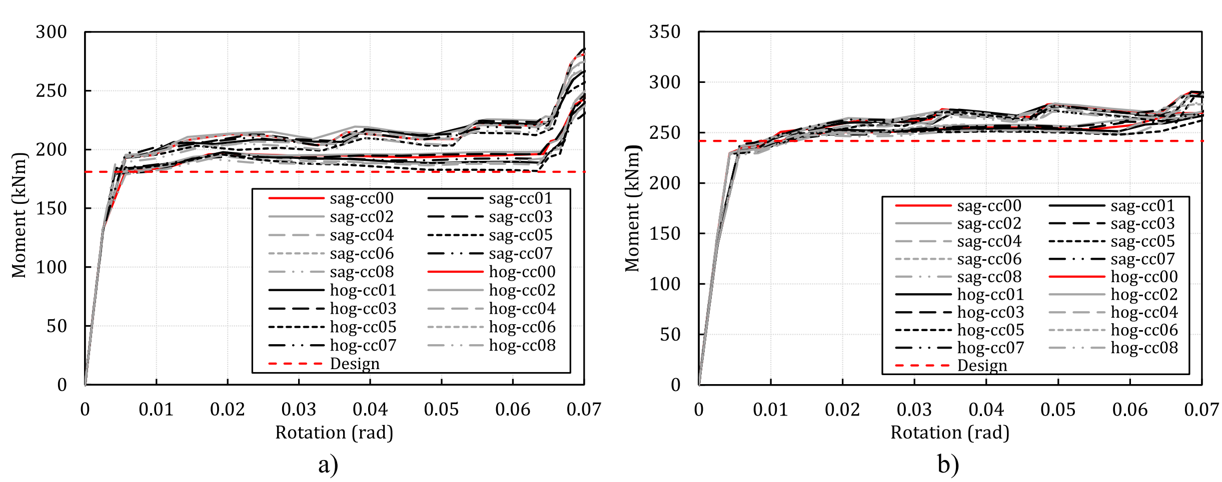

Fig. 21. – Moment-rotation curves in function of the applied clamping loads: a) Configuration D1; b) Configuration D2.

deformation of the system.

The parametric investigations on the preload imperfections highlighted that the global behaviour of the FREEDAM connections under hogging and sagging bending moment is independent of the preload pattern of the damper bolts, provided that the resultant clamping force on the friction damper is equal to the design value.

CRediT authorship contribution statement

Tudor Golea: Writing – review & editing, Writing – original draft, Validation, Methodology, Investigation, Formal analysis, Conceptualization. **Roberto Carlevaris:** Writing – original draft, Validation, Methodology, Investigation, Formal analysis. **Roberto Tartaglia:** Writing – review & editing, Writing – original draft, Supervision, Methodology, Conceptualization. **Mario D'Aniello:** Writing – review & editing, Writing – original draft, Supervision, Conceptualization. **Massimo Latour:** Writing – review & editing, Supervision, Resources, Conceptualization. **Vincenzo Piluso:** Writing – review & editing, Supervision, Resources, Conceptualization. **Raffaele Landolfo:** Writing – review & editing, Supervision, Conceptualization. **Jean-François Demonceau:** Writing – review & editing, Writing – original draft, Supervision, Methodology, Conceptualization.

Declaration of competing interest

The authors declare that they have no known competing financial interests or personal relationships that could have appeared to influence the work reported in this paper.

Acknowledgements

The work presented in this paper was carried out within the DREAMERS demonstration project (GA n°: 101034015). Financial support from the European Commission within the Research Fund for Coal and Steel is gratefully acknowledged.

Data availability

Data will be made available on request.

References

[1] CEN, Eurocode 1: Actions on Structures - Part 1–7: Accidental Actions, European Committee for Standardisation, Brussels, 2006.
[2] J.-F. Demonceau, Steel and composite building frames: Sway response under conventional loading and development of membrane effects in beams further to an exceptional action, PhD Thesis, Université de Liège, Belgium, 2008.
[3] U. Kuhlmann, Redundant and Robust Frame Structures by Joint Ductility, presented at the COST Action TU0601, 1st Workshop, Zurich, Switzerland, 2008, p. 14.
[4] J.-F. Demonceau, J.-P. Jaspart, Experimental test simulating a column loss in a composite frame, Adv. Steel Constr. 6 (3) (2010) 891–913.
[5] B.A. Izzuddin, A.G. Vlassis, A.Y. Elghazouli, D.A. Nethercot, Progressive collapse of multi-storey buildings due to sudden column loss — Part I: simplified assessment framework, Eng. Struct. 30 (5) (2008) 1308–1318, https://doi.org/10.1016/j.engstruct.2007.07.011.
[6] I. Marginean, Robustness of moment steel frames under column loss scenarios, PhD Thesis, Politehnica University of Timisoara, Romania, 2017.
[7] B.A. Francavilla, M. Latour, G. Rizzano, J.-P. Jaspart, J.-F. Demonceau, On the robustness of earthquake-resistant moment-resistant frames: influence of innovative beam-to-column joints, Open Constr. Build. Technol. J. 12 (2018), https://doi.org/10.2174/1874836801812010101.
[8] V. Piluso, et al., Seismic design of steel structures with FREE from DAMage Steel Connections, 1st ed, ECCS – European Convention for Constructional Steelwork, 2022. https://www.steelconstruct.com/wp-content/uploads/FINAL-FREEDAM-PLUS-BOOK-ENGLISH-VERSION.pdf.
[9] M. D'Antimo, Impact characterization of innovative seismically designed connections for robustness application, PhD Thesis, Université de Liège, Belgium, 2020, https://orbi.uliege.be/handle/2268/246289.
[10] A.F. Santos, A. Santiago, M. Latour, G. Rizzano, Robustness analysis of steel frames subjected to vehicle collisions, Structures 25 (2020) 930–942, https://doi.org/10.1016/j.istruc.2020.03.043.
[11] T. Golea, A.F. Santos, J.-P. Jaspart, M. Latour, A. Santiago, J. Demonceau, Design for robustness of steel structures with dissipative FREEDAM joints, Int. J. Earthq. Eng. 2 (2022).
[12] T. Golea, A.F. Santos, J.-P. Jaspart, M. Latour, A. Santiago, J.-F. Demonceau, Robustness of Steel Frame Structures Equipped with FREEDAM Dissipative Joints, ce/papers 5, 2022, pp. 210–217, https://doi.org/10.1002/cepa.1747. no. 4.
[13] R. Tartaglia, R. Carlevaris, M. D'Aniello, and R. Landolfo, "Steel beam-to-column friction joint under a column loss scenario," Buildings, vol. 14, no. 3, Art. no. 3, Mar. 2024, doi:https://doi.org/10.3390/buildings14030784.
[14] V. Piluso, M. Latour, R. Montuori, E. Nastri, C3 Building of Salerno University Campus: the first builidng with FREEDAM Technology, in: Proceedings of the 11th International Conference on Behaviour of Steel Structures in Seismic Areas, Lecture Notes in Civil Engineering (LNCE), Salerno, Italy, 2024, pp. 431–442, https://doi.org/10.1007/978-3-031-62888-7_38.
[15] EN 1993-1-8, Eurocode 3 - Design of Steel Structures - Part 1–8: Design of Joints, European Committee for Standardisation, Brussels, 2005.
[16] G.F. Cavallaro, M. Latour, A.B. Francavilla, V. Piluso, G. Rizzano, Standardised friction damper bolt assemblies time-related relaxation and installed tension variability, J. Constr. Steel Res. 141 (2018) 145–155, https://doi.org/10.1016/j.jcsr.2017.10.029.
[17] EN 1090–2, EN 1090-2-2018, Execution of Steel Structures and Aluminium Structures. Part 2:Technical Requirements for Steel Structures, 2018.
[18] ISO 6892-1:2009(E), INTERNATIONAL STANDARD ISO 6892-1 — Metallic materials — Tensile testing — Part 1: Method of test at Room Temperature. Switzerland: International Organization for Standardization, 2009.
[19] EN 10088–2: 2005, Stainless Steels Technical Delivery Conditions for Sheet/Plate and Strip of Corrosion Resisting Steels for General Purposes, European Committee for Standardisation, Brussels, 2005.
[20] ISO 898-1:2013, Mechanical Properties of Fasteners Made of Carbon Steel and Alloy Steel — Part 1: Bolts, Screws and Studs With Specified Property Classes — Coarse Thread and Fine Pitch Thread, International Organization for Standardization, 2013.
[21] E. Nastri, M. Latour, O. Pecorari, V. Piluso, Experimental lap-shear tests on friction dampers with single and double slotted holes, Eng. Struct. 308 (Jun. 2024) 117968, https://doi.org/10.1016/j.engstruct.2024.117968.
[22] A.F. Santos, A. Santiago, M. Latour, G. Rizzano, L. Simões da Silva, Response of friction joints under different velocity rates, J. Constr. Steel Res. 168 (2020), https://doi.org/10.1016/j.jcsr.2020.106004.
[23] J.-P. Jaspart, A. Corman, J.-F. Demonceau, Ductility Assessment of Structural Steel and Composite Joints. https://orbi.uliege.be/handle/2268/239363, 2019.
[24] FineLg user''s manual, Nonlinear Finite Element Analysis Program, Edition, 2019.
[25] Abaqus 6.14–4, Dassault Systèmes Simulia Corp, Providence, RI, 2014.
[26] M. D'Aniello, D. Cassiano, R. Landolfo, Simplified criteria for finite element modelling of European preloadable bolts, Steel Compos. Struct. 24 (6) (Jan. 2017) 643–658, https://doi.org/10.12989/scs.2017.24.6.643.
[27] A.B. Francavilla, M. Latour, V. Piluso, G. Rizzano, Design criteria for beam-to-column connections equipped with friction devices, J. Constr. Steel Res. 172 (Sep. 2020) 106240, https://doi.org/10.1016/j.jcsr.2020.106240.